DEVELOPMENT OF AERIAL-GROUND SENSING NETWORK:

ARCHITECTURE, SENSOR ACTIVATION, AND

SPATIAL PATH-ENERGY OPTIMIZATION

A DISSERTATION IN
Electrical and Computer Engineering
and
Engineering

Presented to the Faculty of the University of
Missouri - Kansas City in partial fulfillment of
the requirements for the degree

DOCTOR OF PHILOSOPHY

by
JIANFEI CHEN

B.S., Beijing University of Post and Communication, 2010
M.S., University of Missouri-Kansas City, 2013

Kansas City, Missouri
2019

DEVELOPMENT OF AERIAL-GROUND SENSING NETWORK:

ARCHITECTURE, SENSOR ACTIVATION, AND

SPATIAL PATH-ENERGY OPTIMIZATION

Jianfei Chen, Candidate for the Doctor of Philosophy Degree

University of Missouri-Kansas City, 2019

ABSTRACT

The advent of autonomous navigation, positioning, and in general robotics technologies has enabled the maturity of small to miniature-sized unmanned aerial vehicles (UAVs; or colloquially called drones) and their wide use in engineering practice as a low-cost and effective geospatial remote sensing solution. Meanwhile, wireless sensing network technology (WSN) has also matured in recent years with many applications found in engineering practice. In this dissertation, a novel aerial-ground wireless sensing network (AG-WSN) is developed, which is expected to transform a number of critical geospatial sensing and monitoring practices, such as precision agriculture, civil infrastructure protection, and disaster response. Towards the maximal energy efficiency, three research problems are concerned in this dissertation. First, a radio-frequency (RF) wake-up mechanism is investigated for aerial activation of ground sensors using a UAV platform. Second, the data transmission under wireless interference between the UAV and ground WSN is experimentally investigated, which

suggests practical relations and parameters for aerial-ground communication configuration. Last, this dissertation theoretically explores and develops an optimization framework for UAV's aerial path planning when collecting ground-sensor data. An improved mixed-integer non-linear programming approach is proposed for solving the optimal spatial path-energy using the framework of the traveling-salesman problem with neighborhoods.

APPROVAL PAGE

The faculty listed below, appointed by the Dean of the School of Graduate Studies, have examined a dissertation titled "Development of Aerial-Ground Sensing Network: Architecture, Sensor Activation, and Spatial Path-Energy Optimization", presented by Jianfei Chen, candidate for the Doctor of Philosophy degree, and certify that in their opinion it is worthy of acceptance.

Supervisory Committee

ZhiQiang Chen, Ph.D., Committee Chair
Department of Civil and Mechanical Engineering

Ghulam Chaudhry, Ph.D., Department Chair
Department of Computer Science & Electrical Engineering

Cory Beard, Ph.D.
Department of Computer Science & Electrical Engineering

Yugyung Lee, Ph.D.
Department of Computer Science & Electrical Engineering

Ceki Halmen, Ph.D., P.E.
Department of Civil and Mechanical Engineering

Travis Fields, Ph.D.
Department of Civil and Mechanical Engineering

CONTENTS

ILLUSTRATIONS

Figure Page

TABLES

Table Page

ACKNOWLEDGEMENTS

I wish to express my sincere gratitude to my supervisor, Dr. ZhiQiang Chen, for his guidance, support and encouragement. His knowledge and motivation inspired me in many ways and helped me through the hurdles I encountered during my tenure in the PhD program.

I am also grateful to Dr. Ghulam Chaudhry, Dr. Cory Beard, Dr. Yugyung Lee, Dr. Ceki Halmen and Dr. Travis Fields for serving on my supervisory committee and for their valuable inputs on my dissertation research work.

I would like to thank Shimin Tang, Prativa Sharma, Sameer Aryal, Mostafa Badroddin, who as friends were always willing to help and discuss problems with me.

Finally, and more importantly, I wish to thank my parents, for their support and encourage throughout the years.

CHAPTER 1

INTRODUCTION

1.1 Motivation

Wireless sensing network (WSN) technology has matured in recent years with applications found in many scientific and engineering projects. Many of these applications focus on some ad-hoc tasks, and the WSNs are deployed with a goal of completing the task in a short time. Therefore, the energy consumption is not excessive. However, for deploying WSNs over a geospatially large or spatially complex space wherein the long-term monitoring is desired, both WSN implementation and energy efficiency become the primary challenges. One possible application is sensing in farming land, wherein precision-agriculture practice demands data sensed at different granular (spatial and temporal) scales [1]. Another application scenario is to perform structural health monitoring (SHM) for civil structures that often are massive and spatially complex (e.g. a long-span bridge, tunnels, etc.); and for structures that are critical to the society, sensors and especially WSNs can be added to structures in their lifetime hence achieving 'smart structures'. The continuous health monitoring through these smart-structures WSNs provides stakeholders a basis for ensuring public safety and a ground for decision-making when dealing with emergencies [2].

Towards the application in precision agriculture, the traditional practice relies on sensing data such as space- or airborne imagery for farming decision-making and management [3-5]. However, the high cost and the long revisit period of satellite or

aerial imagery may prevent applying precision agriculture solutions at any location and any time around the world. Images taken by low-altitude remote sensing platforms, such as unmanned aerial vehicles (UAVs or commonly called drones), give the alternative solution in the emerging precision agriculture practice [6-8]. In addition, since microelectromechanical systems (MEMS) technology and particularly the emerging Internet of Things (IoT) sensing technology, have been rapidly improved in recent decades, many researchers have proposed and implemented different ground-based wireless sensors solutions for facilitating precision agriculture [9-13].

In the arena of SHM, the traditional utility has been the use of wired or wireless sensors to obtain in the real-time the response of structures due to environmental or hazards-induced vibrations [14-17]. Upon the archival of response data, most SHM technologies then employ signal processing and system identification methods with a goal of characterizing the intrinsic states of the structures. In reality, however, for structures with slight to moderate damage, such as local cracking and corrosion, visual or remote sensing based inspection is the most efficient approach to date. In recent years, as the penetration of UAV technology into many industrial sectors, small-UAVs enabled remote sensing, which is low-cost and highly mobile, is being treated as an emerging tool that expands the SHM technology inventory [18-20]. In recent years, many researchers envision the deployment of SHM to an urban scale for the grand goal of community resilience, for which all critical civil structures and infrastructure systems need to be monitored in coping with life-cycle maintenance or abrupt emergencies [21]. This further corroborates the necessity of combining WSNs and remote sensing

technologies.

Reflecting on the trends in precision agriculture and SHM, we have proposed and developed a prototype of realizing a wireless aerial-imaging and ground-sensing network; or in short, aerial-ground wireless sensing network (AG-WSN). This prototype has the capability of capturing both high-resolution imagery and real-time ground data at the same time. For the two application scenarios described above, Figure 1.1 provides the conceptual illustrations for precision agriculture and city-scale SHM, respectively. First, this AG-WSN features the use of one or multiple UAVs as the primary imaging nodes, which in the meantime serve as the gateway to the ground sensors; second, the wireless sensing units are deployed (by UAV delivering or manual installation) in the ground (or ground structures) over a geospatially large or a spatially complex space. The combination of the low-altitude imaging and ground sensing provides the power of fusing remotely captured images with high resolution and point-based ground-truth data in the field. The high-mobility of the UAV can be deployed opportunistically according to the tasks scheduled or emerged unexpected urgencies (e.g. disasters). Combining the collaborative aerial and ground sensing and the opportunistic operation modes, we state that the proposed AG-WSN can potentially provide the most high-fidelity and most flexible sensing solution to many monitoring problems arising from the need of assessing geospatially large and complex built/agriculture environments. The dissertation work focuses on developing solutions for the above problems. The work contains three major effort, described as section 1.2 through 1.4.

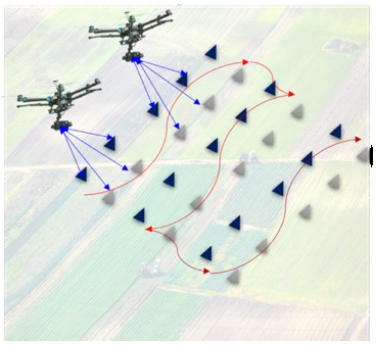

(a)

(b)

Figure 1.1 Conceptual illustrations of the proposed aerial-ground wireless sensing network (AG-WSN) for field monitoring: (a) largely 2-D terrain field in an agriculture setting; and (b) complex 3D field in an urban setting.

1.2 Energy Optimization for Sensor Network

Although solar power or other intermittent energy-supply techniques exist, battery power is continued being considered as the most reliable source for powering sensors and robots. By implementing the commonly adopted duty-cycle method, wireless sensor nodes could be pre-programmed to wake up and communicate with the gateway, then go back to sleep after communicating. This approach for extending battery life has been treated as a default function in many commercial wireless sensors. Researchers also try to optimize the power management to further extend the battery life of WSNs [22-25]. However, one key problem that prevents us from realizing a long-

term aerial-ground sensing is the opportunistic nature of deploying the UAV (gateway) and the sensor notes. In an AG-WSN, the gateway (as a payload of the UAV) is deployed to approach to the ground sensors on a non-scheduled basis or randomly upon the abrupt events. This further implies that the ground sensors do not have 'knowledge' or are not programmable to realize the duty-cycle sensing. If the ground sensors are turned on at least including the microcontroller / communication units (whereas the sensing units may be on or off according to the duty cycles), the battery of the sensor nodes may be drained quickly.

One straightforward approach to such energy inefficiency issue is to wake up ground sensor nodes when the UAV is deployed as needed to approach to the sensors without any preprogramming. In the dissertation, we first propose to use a radio-frequency (RF) based out-of-band wake-up mechanism. Then comparative studies are conducted to investigate their energy saving performance against two other wake-up mechanisms. Using a traditional star-like sensor network, the analytical and experimental studies show solid evidence that the RF-based wake-up mechanism outperforms traditional duty cycle solution and infrared-based wake-up solution on energy consumption.

1.3 Wireless Interference in AG-WSN

It is noted that modern UAVs are often equipped with communication modules and can further carry sensing and routing payloads. This provides the technical feasibility of incorporating UAVs into a WSN that networks with regular ground-based

sensors. On the other hand, the potential of integration UAVs into a WSN is also corroborated by a critical challenge in deploying practical WSNs in challenging environments. For instance, since sensors are usually battery-powered, field sensors are often deactivated and in the 'sleep' mode. Moreover, in a harsh environment or circumstance such as in disaster scenes where cellular networks are crippled, data may become ultimately inaccessible even if a local WSN survives. These challenges can be overcome by taking advantage of the aerial mobility of the UAVs. One solution is to use a UAV to fly to the overhead of the ground WSN, and activate the sensors in an as-needed basis hence achieving maximum energy efficiency [26]. To access data from a ground WSN, the UAV may serve as a gateway to receive data from the ground sensors. It is noted that the concept of integrating UAVs into a WSN or realizing dynamic relay of communication has been similarly proposed by different researchers [27, 28]. However, no physical prototype or applications of such networks to civil infrastructure monitoring is found to date.

Recognizing the potential promise of integrating UAV-based imaging and ground-based WSN in improving the efficiency of collecting civil structures, in our AG-WSN, the UAV is adapted to achieve two immediate roles – as an imaging sensor providing overhead imagery and as a gateway (or data sink) that commands and receives data from the ground sensors. In an earlier effort of the my work [29], the concept of aerial-imaging and ground-sensing was proposed for use in the situation of disaster response in a geospatially wide area. In the dissertation, this concept is borrowed towards structural monitoring at a geospatial scale as well, wherein the health

and conditions of a single large-scale structure or clustered structures (e.g. in a wide area such as a city block) are the concern. In recent years, it is noted that small UAVs are further investigated for the use in an interior or GPS-denied environment with the assistance of machine-vision based navigation [30, 31]. This implies that the proposed AG-WSN may be further extended into use in these challenging environments.

Given such promise and towards deploying the proposed AG-WSN, however, one practical issue that remains not fully resolved is the interference between the UAV's and the WSN's operating frequencies. In practice, most UAVs use 2.4 GHz radio for flight control and 2.4 GHz Wi-Fi (802.11 g/n/ac) for imagery data feeds. For low-power sensing, ground-based WSNs often use the ZigBee (802.15.4) protocol, which may run at 2.4 GHz as well. In the dissertation, an AG-WSN prototype using commercial components is developed, and then the interference issue is experimentally studied.

1.4 UAV Path Planning in AG-WSN

The most traditional and reliable way for wireless sensing network (WSN) method to collect sensing data is using a stationary gateway with multi-hop routing [32]. In some conditions, however, it is not possible nor efficient to using such topology due to the environment and energy restriction. The alternative method is using mobile robotic as the gateway to collect data from the sensor nodes either in multi-hop routing [33, 34], or star topology [35-37]. Unmanned aerial vehicle (UAV) is the perfect mobile gateway for WSN thanks to its high mobility. The UAV will visit all the n sensor nodes in the field once and only once in one trip to gather the sensing data through wireless

communication. The communication range between the UAV and sensor nodes is limited by many factors like power, obstacles and antenna directions. This require the UAV get close within the area Qi of each sensor node i. The UAV then will hover at each point qi ∈ Qi of node i = 1,2…n for data collecting. limited UAV battery life requires the UAV reaching out all the sensor nodes on the ground with the shortest path to save energy.

This path planning for the UAV falls into category of Travelling Salesman Problem with Neighborhood (TSPN), which was introduced by [38]. Early researchers use small fixed wings to retrieve data [39]. Due to the nature of fixed wings, Dubins Travelling Salesman Problem with Neighborhood seems fit this situation well and has been studied for a while [40-42]. The downsides of these fixed-wing UAVs are: a) They need a small airstrip to take off. b) They cannot hover above the sensor nodes, thus collecting data require them to flying around which makes wireless communication more difficult. Fortunately, with the development of new technology in Multi-Rotor UAV, the above two problems can be solved. Therefore, the Multi-rotor UAV is the perfect mobile gateway for WSN.

Traditional TSPN optimization aims to provide the shortest Euclidean distance solution to visit all the neighborhood, since shorter path equals less time and energy consumed by the salesman (which is UAV in WSN application). The research focus is the energy optimization for UAV in the TSPN problem, since the UAV will stay hovering during the communication with sensor node, and the energy consumption to maintain hovering is almost identical to moving around [43], therefore, the energy

consumed during this hovering time must be taken into consideration when optimizing the path. Thus, the shortest Euclidean path does not necessarily mean the lowest energy consumption for the UAV. Traditional TSPN problem is already NP-hard, in practical, the energy of the UAV system is consumed by multiple sources like motors, on board computing units and wireless communication module, which makes the problem even harder to solve. To simplify the problem, we focus on the major energy consumption activity of the UAV, moving and hovering. In this dissertation, we modify existing TSPN solution and use mixed-integer non-linear programming method to minimize the total energy consumption of the UAV, by considering both energy consumed during Euclidean distance traveling, and energy consumed when UAV is hovering for wireless communication.

CHAPTER 2

DEVELOPMENT OF RADIO-FREQUENCY SENSOR WAKE-UP THROUGH UAV AS AN AERIAL GATEWAY

2.1 Introduction

With advances in autonomous navigation, positioning, and in general robotics technologies, small to miniature-sized unmanned aerial vehicles (UAVs; or colloquially called drones) are witnessing their ever-increasing use in engineering practice, due to a simple fact that they are much low-cost, agile and effective, particularly for geospatial remote sensing platform when compared with traditional space- or airborne remote sensing [44]. Today's UAVs have well adopted the latest GPS technology; and many small UAVs, especially the multi-motor ones can fly following the predetermined GPS waypoints. Some advanced drones have been equipped with lost-cost radar or vision sensors acquiring a minimum level of flying beyond (visual) line-of-sight (BVLOS or BLOS) due to its sense-and-avoid capability [45-47]. This potentially would further render small UAVs an attractive remote sensing platform for a great deal of different applications.

On the other hand, wireless sensing network (WSN) technology has matured in recent years with applications found in many scientific and engineering projects. Many of WSN applications focus on ad-hoc tasks, and the local (contact-based usually ground-based) sensors are deployed with a goal of completing the task in a short time. Therefore, the energy consumption is not excessive. However, for deploying WSNs over a geospatially large or spatially complex space wherein the long-term monitoring

is desired, both WSN implementation and energy efficiency become the primary challenges. One possible application is sensing in farming land, wherein precision-agriculture practice demands data sensed at different granular (spatial and temporal) scales [1]. Another application scenario is to perform structural health monitoring (SHM) for civil structures and life-line infrastructure systems that often are massive and spatially complex (e.g. urban buildings, long-span bridge, and power transmission lines/towers, etc.). For structures that are critical to the society, sensors and especially WSNs can be installed for these structures in their lifetime hence achieving 'smart structures'. The continuous health monitoring through these WSNs provides stakeholders a basis for ensuring public safety and a ground for decision-making when dealing with unexpected damage or losses [2].

Still taking the two arenas of precision agriculture and structural health monitoring as the application setting (Figure 1.1), it is asserted that in both situations, the necessity of combining UAV-based remote sensing and WSNs is straightforward. In the setting of precision agriculture, the traditional practice relies on sensing data such as space- or airborne imagery for farming decision-making and management [3-5]. However, the high cost and the long revisit period of satellite or aerial imagery may prevent applying precision agriculture solutions at any location and any time around the world. Images taken by low-altitude UAVs give the alternative solution in the emerging precision agriculture practice [6-8]. In addition, since microelectromechanical systems (MEMS) technology and particularly the emerging Internet of Things (IoT) sensing technology, have been rapidly improved in recent

decades, many researchers have proposed and implemented different ground-based wireless sensors solutions for facilitating precision agriculture [9-13]. Towards data fusions and more intelligent and tactic operation of these sensing modalities, integration of UAVs and ground-based WSNs becomes a rational choice.

In the arena of SHM, the traditional utility has been the use of wired or wireless sensors to obtain in the real-time the response of structures due to environmental or hazards-induced vibrations [14-17]. In reality, however, for structures with slight to moderate damage, such as local cracking and corrosion, visual or remote sensing based inspection is the most efficient approach to date. In recent years, as the penetration of UAV technology into many industrial sectors, small-UAVs enabled remote sensing, which is low-cost and highly mobile, is being treated as an emerging tool that expands the SHM technology inventory [18-20]. This further corroborates the necessity of combining WSNs and UAV-based remote sensing technologies.

Reflecting on the trends in precision agriculture, SHM and other field applications for critical missions, we have proposed and developed a prototype of realizing a wireless aerial-imaging and ground-sensing network; or in short, aerial-ground wireless sensing network (AG-WSN) [48]. First, this AG-WSN features the use of one or multiple UAVs as the primary imaging nodes, which in the meantime serve as the gateway to the ground sensors; second, the wireless sensing units are deployed (by UAV delivering or manual installation) in the ground (or ground structures) over a geospatially large or a spatially complex space. The combination of the low-altitude imaging and ground sensing provides the power of fusing remotely captured images

with high resolution and point-based ground-truth data in the field. The high-mobility of the UAV can be deployed opportunistically according to the tasks scheduled or emerged unexpected urgencies (e.g. disasters). Combining the collaborative aerial and ground sensing and the opportunistic operation mode (e.g. a ground node may be only active when the UAV hovers above it and collects data from it), we state that the proposed AG-WSN can potentially provide the most high-fidelity and most flexible sensing solution to many monitoring problems arising from the need of assessing geospatially large and complex built/agriculture environments.

In this paper, first, addressing the opportunistic nature of the AG-WSN, we first review the related UAV-WSN integration efforts and propose a conceptual operation design, which further motivates the proposition of sensor activation for network energy efficiency. Centering around sensor activation, we propose to develop a sensor wake-up solution, and the related work is provided that shows the benefits and drawbacks of different wake-up design and the rationale for choosing an active RF mechanism. Subsequently, a general out-band wake-up mechanism is developed and demonstrated. For a comparative purpose, the infrared wake-up prototype is implemented too. We further conduct a comprehensive study of the energy consumption on how much energy can be saved, followed by the conclusions and remarks of this paper.

2.2 Opportunistic Sensing, and Research Needs

To our best knowledge, there were only a few efforts that attempted to integrate UAVs with wireless sensor networks. In [27], UAVs are considered as mobile sinks for ground sensor data dissemination. This approach intends to optimize the route from a

given sensor node on the ground to a few mobile sinks that move in the area. [28] presents a different approach that keeps the sensor network continually connected. It uses multiple UAVs to establish a reliable relay network to guarantee the delivery of data produced by the wireless network nodes on the ground to the users. Given these few simulation-based and conceptual efforts, much fewer efforts are found to physically realized UAV-based sensing network system. In a recent effort, the authors developed a WSN using a fixed-wing UAV as the aerial gateway for marine data collection [49]. In our recent effort, we further investigated the interference between the WiFi-based video transmission link and the ZigBee-based ground-data transmission links [48].

The use of flying single or multiple UAVs either as a mobile sensor node or a data sink triggers the effort of optimizing network efficiency between sensors and sinks, among which energy cost is an inevitable constraint considering that both the UAVs and ground sensors are usually battery-powered to this date. Opportunistic Network is the emerging technology that solve such optimization problem. In [50], it proposes protocols to better exploit durations of high-quality channels condition. Based on that, [51] proposed routing protocols that increase the throughput of large unicast transfers in multi-hop wireless network. There are also research efforts on optimizing resource and performance in wireless sensor networks (e.g. [52]). It considers a different scenario where the paths from message sources and their destinations do not always exist. Then the authors analyzed protocols that alleviate the problem of chronically disconnected paths by having a node storing the packet, carrying it until meeting another relay node, and forwarding the packet to the other relay node. In a more recent

effort, researchers also developed middleware that implemented the opportunistic network into mobile social networks, called CAMEO [53]. It is stated that these optimization schemes mostly focus on designing improved communication protocols by assuming that either the UAVs or the sensors are not constrained by the battery-based power. It is noted that in general opportunistic networking (without using a UAV as a gateway node), different protocols are proposed, including the flooding protocol and the history-based protocol (e.g. [54, 55]).

To illustrate such energy constraint, Figure 2.1 illustrates a conceptual AG-WSN, where besides being the imaging and computing hub, the UAV is designed as a robotic vehicle that flies to ground sensors at tactic locations. This operational mode, and furthermore, the possible loss of sensors, sensor malfunctions, and out-of-range communication render the underlying networking opportunistic, which in the meantime affects energy assumption in the UAV and the sensors.

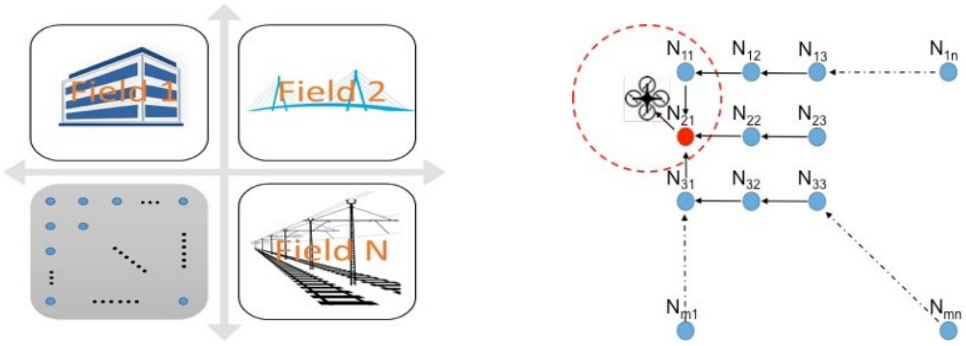

(a) (b)

Figure 2.1 Conceptual field development of an AG-WSN and opportunistic networking.

In Figure 2.1(a), four subnets are shown, which indicate four physically isolated sensor networks in the fields, except that the UAV can fly to each subnet to execute opportunistic sensing. Figure 2.1(b) indicates the idealized situation where sensor

failure (or other malfunctions) and energy consumption are not needed to consider. Hence, assuming each node N_{ij} can communicate with its neighboring nodes $N_{i\pm1,j\pm1}$ through wireless connection, when the UAV fly into this sub-network, some of the nodes are in communication range to the UAV, while some are not. The UAV will pick one of the nodes in the range as a relay node, and collect data from any other node in this subnet. Then the existing optimal communication protocols can be used.

When the energy consumption of either the UAV or sensor networks are considered, optimization in the physical layer (rather than in the communication protocols) need to be addressed. Two obvious venues exist: (1) through spatial path-energy optimization, the UAV finds the optimal flying path through the geospatially deployed ground sensors, for which it is being tackled in Chapter 4 of this dissertation; and (2) as being concentrated in this paper, through a sensor activation approach, as such the sensors are only active when the UAV is in its neighborhood.

2.3 Sensor Activation and Related Work

Although solar power or other intermittent energy-supply techniques exist, battery power is continued being considered as the most reliable source for powering sensors and robots. By implementing the commonly adopted duty-cycle method, wireless sensor nodes could be pre-programmed to wake up and communicate with the gateway, then go back to sleep after communicating. This approach for extending battery life has been treated as a default function in many commercial wireless sensors. Researchers also try to optimize the power management to further extend the battery life of WSNs [22-25]. However, one key problem that prevents us from realizing a long-

term aerial-ground sensing is the opportunistic nature of deploying the UAV (gateway) and the sensor notes. In an AG-WSN, the gateway (as a payload of the UAV) is deployed to approach to the ground sensors on a non-scheduled basis or randomly upon the abrupt events. This further implies that the ground sensors do not have 'knowledge' or are not programmable to realize the duty-cycle sensing. If the ground sensors are turned on at least including the microcontroller / communication units (whereas the sensing units may be on or off according to the duty cycles), the battery of the sensor nodes may be drained quickly.

One straightforward approach to such energy inefficiency issue is to wake up ground sensor nodes when the UAV is deployed as needed to approach to the sensors without any preprogramming. In this paper, we first propose to use a radio-frequency (RF) based out-of-band wake-up mechanism. Then comparative studies are conducted to investigate their energy saving performance against two other wake-up mechanisms. Using a traditional star-like sensor network, the analytical and experimental studies show solid evidence that the RF-based wake-up mechanism outperforms other two solutions on energy consumption.

Earlier efforts reveal that data transmission in a WSN is generally very expensive in terms of energy consumption, whereas data collection (or the sensing itself) consumes significantly less [56]. For this reason, various methods are developed to extend the life of battery-powered WSNs by reducing the power consumption of the wireless modules. A significant number of efforts were found that focused on developing lower-level network protocols by adopting duty-cycle based solutions [57-

59]. These studies aimed to optimize the network protocols, specifically through reducing the energy consumption during the idle or the listening time of the wireless modules. For example, the authors in [60] proposed an adaptive Medium Access Control (MAC) protocol, which introduced a flexible duty-cycle method and claimed to reduce 96% of energy use compared with traditional protocols. However, the core concern for these duty-cycle solutions is that the wireless modules do not know when the data transmission is coming or required, the node must listen periodically to limit data latency, thus the duty-cycle ratio cannot go arbitrarily low [61]. Also, duty-cycle methods may have problems with delay and synchronism; and hence the protocol is relatively complicated. As such, the waking-up mechanisms as an answer to this concern have been extensively studied.

Different sensor activation methods were proposed to date. Essentially, such activation approach features a waking-up mechanism for activating sensing modules in an as-needed (or on-demand) basis. There are two methods when considering wake-up mechanisms for use in wireless networks, which are in-band and out-band. If an in-band method is used, a special value is transmitted through the data channel to send out the wake-up signal. By contrast, a separate channel is needed to realize such waking-up mechanism in an out-band method. Using the in-band methods can reduce the complexity and cost of the implementation. A recent study of the in-band wake-up method [62] claimed that by using both game theory and reinforcement learning techniques, it achieved very effective sleep/wake-up scheduling. However, it keeps the wireless communication channel busy and may require more energy consumption.

From the energy-efficiency perspective, the out-band approach suits more for the proposed concept that emphasizes opportunistic aerial-ground sensing.

There are many studies that employ the out-band wake-up mechanism [63]. In this paper, they are categorized into two groups according to their communication medium: (1) non-RF based and (2) RF-based. In a non-RF based mechanism, researchers proposed wake-up methods using infrared (IR), optical and acoustic signals. The authors in [64] developed an IR LED based wake-up mechanism, in which the receiver is a photo-detector receiving IR signal and then generate an interrupt. The authors stated that the IR design only consumed 12 μW while listening. It is noted that the obvious drawback of this prototype is its circuit's sensitivity to external light and vulnerability to ambient noise. In [65], the authors presented a home-energy management system using infrared signal-based control over a Zigbee network. In this system, an infrared receiver is attached to the Zigbee gateway. The Zigbee gateway is responsible for communicating with other home appliances, whereas the infrared remote control is the out-band wake-up channel used to wake up the Zigbee network. Unfortunately, this paper did not mention the power consumption of the IR receiver. To our understanding, this type of IR receiver in the paper is commercially available and similar to the one used in our experiment as shown in this paper, which has better resistance to noise at a cost of much higher power consumption and may require up to 45 mW according to our experiment.

Optical communication is another non-RF option for the secondary wake-up channel. Both [66, 67] used free-space optical (FSO) communication as the transceiver.

The receiver at idle-listening consumes 317 μW and 695 pW. However, the transceiver and receiver both need to be placed line-of-sight (LOS) and the data rate is slow. It is impractical for use in a UAV that mostly time does not stay in position to accurately face the transmitter. Thus, this option is not suitable for our application. The AG-WSN scenario may also limit the use of acoustic as wake-up methods [68, 69] due to the noise produced by the UAV blades. Ultrasonic, as stated in [70, 71], may avoid the noise made by the UAV. It uses a piezoelectric transducer that converts the mechanical energy into electrical energy for generating wake-up interrupts. However, most ultrasonic communication or ranging efforts to date are mostly applied to indoor (short-range) or LOS scenarios [72, 73] .

Compare with the non-RF based wake-up mechanisms reviewed above, first of all, the RF-based communication has the advantages of not requiring LOS, better noise and interference tolerance, higher data rate, and is more cost-effective. The research endeavors on the RF-based wake-up mechanism can be divided into two designs: passive wake-up and active wake-up, both of which have been well studied in the laboratory environment. In a passive design, the RF receiver harvests energy from the transmitter to power itself thus requires no power supply [74-76]. In [77], it simulated a passive RF wake-up receiver, in which the authors indicated that comparing with the existing duty-cycle method, their RF wake-up can significantly enhance energy efficiency by up to 70%. There are also simulation endeavors on both passive and active RF wake-up circuits, such as [78, 79]; the authors of these efforts later implemented the passive RF circuit into a sensor network with a multi-hop capability [80]. However,

among these passive RF-based methods, information on the communication range between the transceivers was not found. In addition, it was reported that the energy of the receiver harvests may decrease with increasing distance between the receiver and the transmitter. The authors in [81, 82] showed that the hardware setup can only reach a maximum distance of 4 meters for a successful wake-up. Considering the AG-WSN scenario proposed in this work, it is stated that the passive RF-based wake-up is not suited.

Regarding the active RF wake-up design, as mentioned in [61], there are 13 active RF-based wake-up methods using discrete components, whereas there are 29 methods using CMOS technology. The most significant parameters relevant to these designs and prototypes for the interest of the proposed AG-WSN configuration are power consumption, range, address decoding capability, wake-up latency, and their balancing. For example, the author in [83] configured the wake-up receiver using discrete components and claimed to achieve 120 meters of communication range. However, the receiver consumes 1620 μW at the state of idle-listening, which is too high for the battery-powered nodes. There is a low-power design in [84], which only consumes 52 μW; unfortunately, the authors did not provide a range test. A favorable design was presented in [85] recently. It achieved a communication range of 50 meters at idle-listening with a power consumption of 1.2 μW. Unfortunately, at the time of our experiment, there was no market-ready product or porotype based on this design.

In this paper, it is stated that the use of off-the-shelf components is stressed in our prototyping and experimental validation with the goal of putting the proposed AG-WSN into practice rapidly. As many researchers similarly used, the AS393X wake-up receiver has been used in many efforts and designs [86-90]. Among these researches, the author in [89] used AS3933, which is the same chip in our experiment, to prototype the receiver circuit to have an 87-meter communication range, at the cost of more than 5000 μW power consumption when decoding the wake-up signal. Also, in a recent paper, the authors compared the RF wake-up mechanism and the low-power listening techniques [91] and concluded similarly what we achieve in our energy evaluation results in this paper. However, the authors of this paper did not measure the delay caused by the RF wake-up transmission, and their power consumption measurement was not based on battery but a constant power supply, hence lacking a realistic configuration.

2.4 Proposed Energy Efficient Sensing Network

2.4.1 Topology and Implementation

In our aerial-ground approach, the UAV is the wireless network gateway, which is responsible for communicating with each individual sensor node that is deployed in the field. Although there are many wireless protocols that can be configured for these sensors nodes, we choose XBee (a modified Zigbee wireless protocol) wireless module for constructing the network, since its power consumption is relatively low. The XBee

protocol allows three types of network topologies, which include: star, mesh, and cluster-tree. Although mesh and cluster-tree networks have a very flexible network structure, they both require some sensor nodes in the network for relaying data to the gateway, which means that these relay nodes have to be either always active or being duty-cycle active, further consuming a significant amount of power. Alternatively, the star topology does not require any node to relay information, and they can be kept in sleep modes for most of the time. When using the star topology, the UAV will be the XBee coordinator (gateway) for collecting data from multiple ground nodes in the communication range. More importantly, it is the high-mobility UAV that will wake up multiple ground sensor nodes from the sleeping state on the demand of the UAV, which can fly to the overhead of individual or a group of sensors to perform sensor activation and data collection. Therefore, the star topology is considered the most appropriate one for the proposed aerial-ground network.

One concern is that using UAV as a flying gateway may consume more energy per a UAV flight than what could potentially be saved in our wake-up mechanism. The fact is that in most cases, the batteries in sensor nodes are hard to replace due to a variety of reasons, such as the position of the node is difficult to reach, or battery is sealed in a box and buried in soil or structures to prevent harsh weather conditions. The key concept of our approach is to reduce the consumption of the sensor-node batteries in the field as much as possible to sustain service time as long as possible. For the power consumption, we state that in reality multiple identical UAVs with multiple high-capacity battery backups can be used to perform their functions of remote sensing and

being the network gateway.

Last, for implementing the sensing nodes, we use Libelium's Waspmote® as our ground sensing nodes [92]. The Waspmote sensing node contains a low-power MCU, embedded sensors, and optional wireless module slots. It consumes a quite small amount of energy when its sleeping mode is selected.

2.4.2 General Active Out-band Wake-up Mechanism

As reviewed earlier, active out-band wake-up mechanism is chosen for the proposed AG-WSN. To understand this mechanism, Figure 2.2 summarizes the state and action diagram for the wake-up mechanism and the sensor-node operation. A description is given as follows:

1) When the sensor node is deployed in the field, it is pre-programmed with a duty-cycle sensing schedule, then it is turned into sleep mode, which we call the initial state. Only the wake-up receiver is listening, in our example, which is either an infrared or RF wake-up receiver.
2) If a wake-up signal is received by the sensor node, it will check whether the signal matches the pre-stored pattern. If not, the node ignores the signal and changes back to the initial state.
3) If the wake-up signal matches the stored pattern, the node wakes up, starts the XBee module, and turns off the wake-up receiver. Then the XBee begins scanning the gateway on the UAV.
4) If the XBee module fails to find the gateway in a couple of tries, the node shuts down the XBee module and turns back into the initial state.

5) If the XBee module is successfully connected to the gateway, it starts the communication with the UAV as programmed (e.g. sensing data or updated schedules).

6) After the communication ends, the node again turns into the initial state.

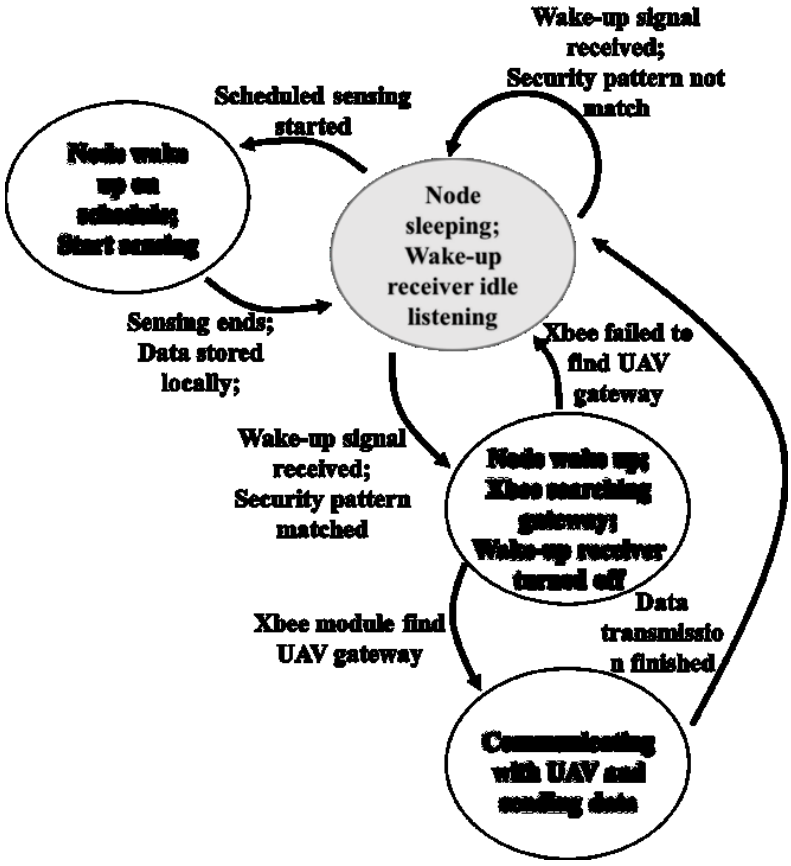

Figure 2.2 State and action diagram of the ground sensor nodes and the UAV.

2.5 RF and Infrared Mechanisms and Implementation

2.5.1 Proposed RF Design and Implementation

The RF wake-up approach is the latest innovation towards achieving energy saving for wireless networks. There are two types of implantation methods: (1) the method that uses active wake-up receivers and utilizes energy from a battery, and (2) the method that uses passive wake-up receivers and harvests energy from the wake-up

radio. In our approach, we find that active wake-up receivers have much better performance in range and a higher rate of success in changing between listening and wake-up modes. In addition, the energy consumption for the RF receiver can be as low as serval μW while it is in its listening state. Figure 2.3 summarizes the RF-based wake-up design proposed in this paper.

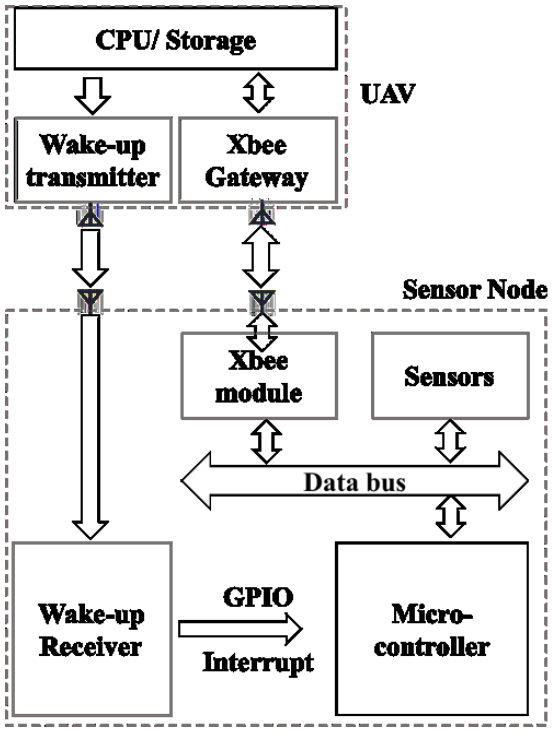

Figure 2.3 Design for the RF-based active wake-up mechanism

To implement the design in Figure 2.3, we choose to use a commercial product, AS3933, as the wake-up receiver, which is further attached to the Waspmote sensor node. AS3933 is a 3-channel low power amplitude-shift-keyed (ASK) receiver,

which is able to generate a wake-up signal upon detection of a data signal that uses an LF carrier with a frequency range of 15-150 kHz. The receiver's output is connected to the MCU's interrupt pin at the sensor board. When the AS3933 receives an RF signal, it decodes and checks whether the signal matches the pre-stored pattern.

Once confirmed, the receiver will send out a pulse to the interrupt pin to wake up the MCU. Figure 2.4(a) shows the hardware setup of the three components in our RF wake-up prototype.

By adding the RF antenna to the UAV and programming the micro-controller on the UAV to generate a Manchester wake-up pattern, we can use the UAV as a control hub to wake up sensor nodes in the range. Since the MCU is in sleep mode using this out-band wake-up method, one interesting question is how much time it would cost from sending out the wake-up signal until the MCU wakes up. If this procedure takes significant additional time, then we need to consider this delay as a drawback for this RF wake-up mechanism. This potential pitfall is carefully studied in this paper.

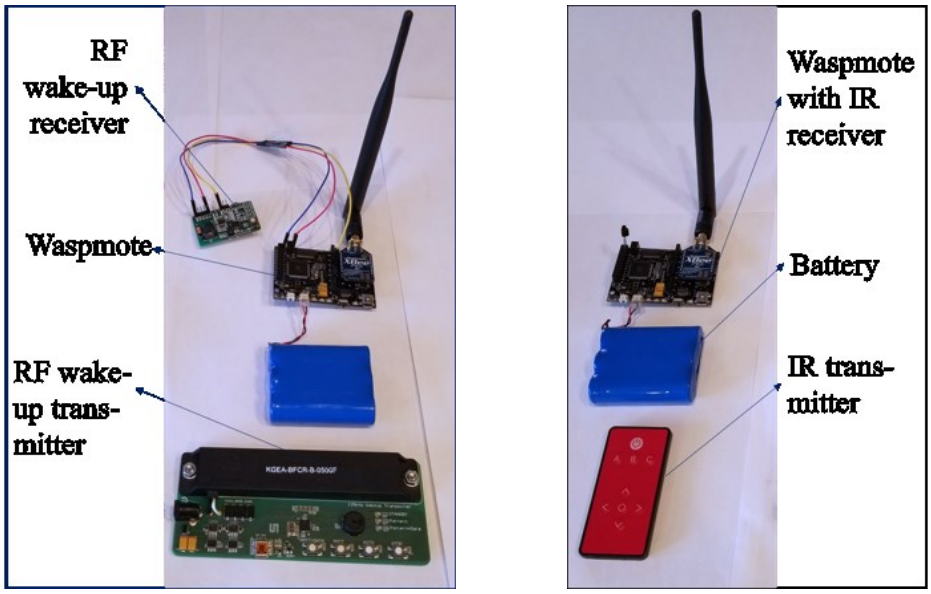

(a) (b)

Figure 2.4 Hardware components of the two wake-up systems: (a) RF wake-up; and (b) Infrared wake-up.

2.5.2 Infrared Wake-up Implementation

To achieve a comparative setup to justify the proposed RF method, the infrared

wake-up mechanism is too implemented physically in this endeavor. Infrared is a commonly used solution for simple wireless communication at short ranges [63]. There are two basic components in an infrared wireless communication: emitter and receiver. The emitter first transmits the coded data, generated by the micro-controller, to the receiver. When the receiver reads the IR signal, it decodes the signal into digital data and then passes the information to its following component, i.e., the sensor node. In our implementation, we integrate a 950 nm-emitting IR LED onto our UAV, and a TSOP38238 IR Receiver Module on the sensor board; Figure 2.4(b) shows these modules. The emitter is connected to the UAV on board with an MCU's PWM-capable I/O pin, and the receiver is connected to the MCU regular digital I/O pin on the sensor board.

To achieve the wake-up function, the emitter on the UAV will send out the wake-up signal to the receiver, only when the signal matches the code that is stored in the MCU (on the sensor board), the sensor board then turns on its sensors and XBee communication module. In this setup, sensors and XBee module can be turned off until the MCU receives the wake-up signal. However, it requires that the sensor board MCU always stay on to check whether the infrared signal matches the specific pattern.

2.6 Experimentation and Results

In the following, we evaluate the wake-up range as well as the energy consumption for both out-band methods (RF and IR), then compare the energy cost with the traditional duty-cycle method, all based on the same hardware setup.

2.6.1 Physical Verification and Comparison

The RF wake-up, however, does not require a direct LOS. The receiver, AS3933, has three wake-up channels, each connecting to an antenna. In our test, the three antennas were set up perpendicularly. Any antenna received the correct pattern may trigger the wake-up. We tested the wake-up range using the similar method; and we found that to successfully wake up the sensor node, the maximum range was affected by the power supply of the transmitter. In our test, we used a 125-KHz antenna connected to the UAV's MCU and external power supply. When the supply voltage for the transmitter was set to 9 V, the maximum range was around 7 meters in an indoor environment. A similar result in the outdoor test using the same receiver is found in [86], which resulted in a 5-meter range using 12-V supply for the transmitter.

2.6.2 RF Wake-up Delay

Since it takes time for the MCU to wake up from sleeping, we expect that this may cause a delay in the data gathering for the WSN. Other wake-up receiver designs like the one reported in [93] claimed to have a latency of 214 milliseconds; while in [85], the author achieved around 0.9 milliseconds. We want to compare our set up with other wake-up design to make sure the latency value is in an acceptable range. To evaluate this and to measure the time from the transmitter at sending a signal, to the MCU at waking-up and returning to the normal routine, we set up a novel photogrammetric test environment. In the RF wake-up setup, we have three different components, which have been introduced in Figure 2.4(a), the wake-up transmitter, the wake-up receiver, and the MCU. The measurement operates as follows:

1. When the transmitter sends out the wake-up signal, the LED on the

transmitter will flash, the moment at which is defined as t_1.

2. When the receiver receives the signal and decodes it if the signal matches the pre-stored key, then the LED on the receiver will flash, the moment at which is t_2.
3. When the receiver sends out the wake-up trigger to the MCU interrupt pin, then the MCU wakes up and the LED on MCU board will flash (t_3).

We used a high-speed camera (Sony RX100 V) which can record 1000 frames per second to record the above sequence in a video format. By calculating the video frames between each LED lights up, we can obtain the time delay since each frame equals to 1 millisecond. One picture frame of the video is shown in Figure 2.5.

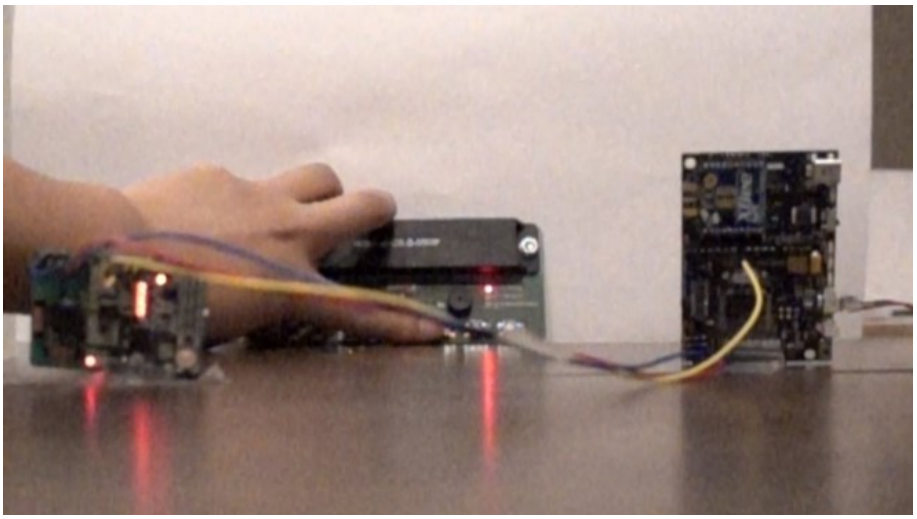

Figure.2.5 One image captured in the high-speed video. In the middle is the wake-up transmitter, the left is the wake-up receiver, and to the right is the MCU. This image is the frame when the receiver decodes the signal and find it matched, thus the LED on the receiver board is lit up.

After the test, we found that the receiver had some failed wake-up instances due to environmental RF noise when simple coding (short pattern) is used. The solution to this would be increasing the wake-up single pattern from 16-bit Manchester coding to

32-bit, or double the wake-up single pattern length. Four coding conditions were considered and tested, and the time intervals between t1 and t2, and between t2 and t3 are recorded. Combining all these coding solutions, the time-delay values averaged from multiple tests are reported in Table 2.1.

Table 2.1 Average time-delay (in terms of milliseconds) within the wake-up procedure

Coding Pattern	Time between t_1 and t_2	Time between t_2 and t_3	Total time-delay
16-bit, Single pattern	12	49	61
32-bit, Single pattern	18	49	67
16-bit, Double pattern	18	49	67
32-bit, Double pattern	31	48	79

The above result reveals that with different coding set up for the transmitter and receiver, first, the time delay between t_1 and t_2 increases when longer-bit Manchester codes or double patterns are transmitted. This is because both transmitting and decoding phases take longer if the coding is more complex. Second, comparatively the delay times between t_2 and $t_{3\ in}$ as shown in Table 2.1 stay almost the same; this is because that t_2 is the time when the wake-up receiver sends out the signal through wiring to the MCU, at which all decoding procedure is already completed. Thus, the delay between t_2 and t_3 only represents the wake-up time of the MCU and will not be affected when

different coding patterns are used.

Regardless, through this experiment, since the total delay caused by using this RF wake-up mechanism is less than 80 milliseconds (from sending out the wake-up signal by the transmitter to the MCU's wake-up), we can safely conclude that this wireless wake-up mechanism will not affect the data communication between the gateway and the sensor nodes in the field for most sensing applications, where the sensors sense data packets at a time and transmit at a different time, then stay idle with much longer duration. The study in [94] claimed to reduce the time between t_1 and t_2 roughly from 13 ms to about 2 ms using 16-bit and single pattern with the similar setup in this paper. We thought this could potentially further reduce the latency introduced by this out-band wake-up mechanism. Another study in [87] using the same chipset claims the time between t_2 and t_3 to be 45.87 ms, which is similar to our experiment.

2.5.3 Energy Consumption Analysis and Verification

The energy consumption is one of the primary concerns of this paper. Our main study focuses on the energy consumption in the sensor nodes that are potentially deployed in the hard-accessible field. Specifically, we classify each sensor module hardware into four sub-units represented by the primary device: the MCU, XBee module, wake-up receiver, and the sensors. In Table 2.2, we list the typical current consumption with a 3.3 V supply voltage for this hardware. We did the comparative experiment on one default (duty-cycle) energy-saving mode and two wake-up mechanisms as we explained earlier, and recorded the power consumption:

1. Solution 1 – the simple duty-cycle method (default in the Libelium

sensor network). In this method, no out-band wake-up method is used. We use the XBee as our data communication as well as the wake-up channel. The XBee module on the sensor node will state in listening mode if no UAV is nearby. Using this solution, the XBee and MCU on the sensor board have to be always turned on.

2. Solution 2 – infrared wake-up method implemented in this paper. The infrared receiver is used as the wake-up channel. Since the IR receiver is connected to the MCU GPIO, it requires MCU always stay on while XBee module can be turned off.
3. Solution 3 – RF wake-up method proposed and implemented in this paper. The RF is used as the wake-up channel. The receiver connected to the MCU's interrupt pin, the MCU will stay in sleep mode. The MCU only costs the current of 55uA while in sleep mode.

Table 2.2 Nominal current values for sub-units within a sensing module.

Hardware	Current
MCU	15mA
Sensors	30mA
XBee	165mA/45mA*
IR	0.45mA
RF	2.3uA
*The two values represent working/idle listening	

We assume the same schedule for the different solutions, in which T_i, T_s, T_{tran}, represent the duration of the idling state, sensing state, and the transmitting state of the sensor node, respectively. Considering 24 hours as a working period, if every 4 hours

the node will sense the data and transmit to the gateway, the value of T_s and T_{tran} in 24 hours are usually less than 10 minutes, whereas the remaining of the time belongs to T_i. This means that the significant part of the power consumption is spent within the T_i period when accumulated with time. Figure 2.6 illustrates the solution's electric current consumption considering the aforementioned typical durations.

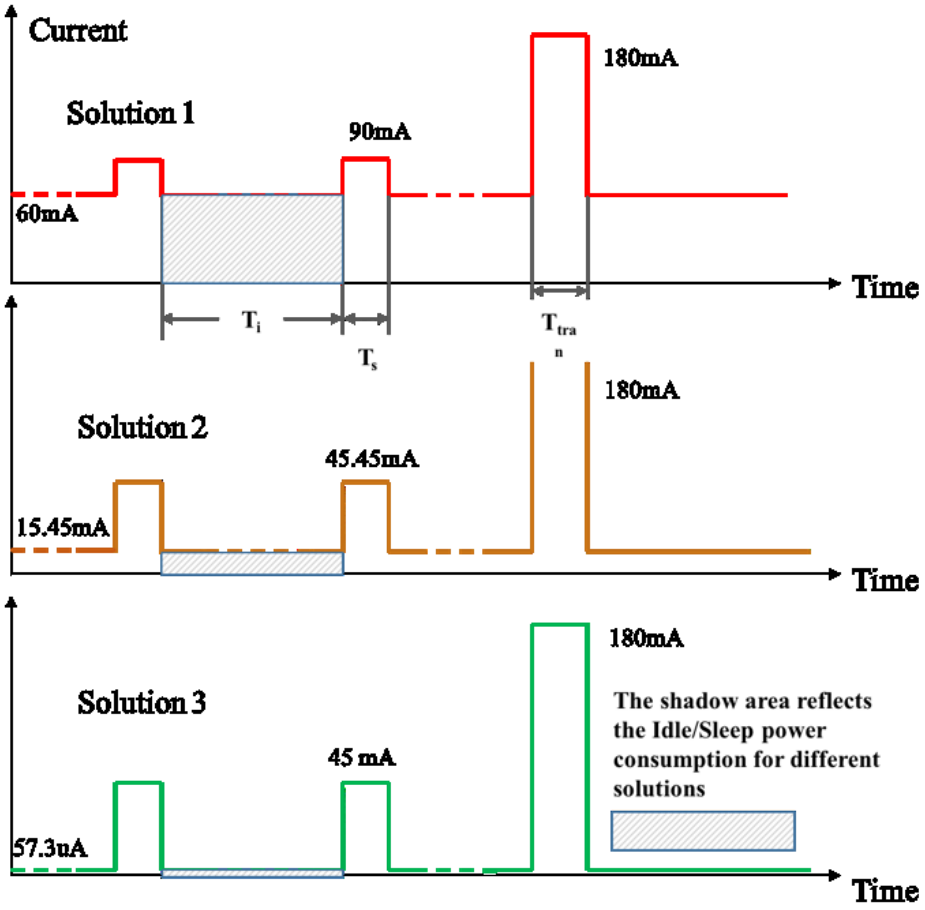

Figure 2.6 Energy consumption illustrations resulting from the three solutions.

The power consumption for one sensing cycle can be calculated by the following formula:

$$E_{cycle} = [T_i \times I_i + T_s \times I_s + T_{tran} \times I_{tran}] V_{dc}$$

where $I_{i,\ s,\ trans}$ is the current variable at the state of idling, sensing, and data

transmitting as defined in Table 2.2, respectively; and the resulting E_{cycle} defines the energy consumption in a designated cycle proportional to the constant battery DC voltage.

Using this formula and the data from Table 2.2, we can qualitatively state that the Solution 3 needs much less energy for the idle state. By simple algebraic calculation based on Table 2.2 and the assumed typical idling (4 hours), sensing duration (1 min), and transmitting duration (1 min), the Solution 3 costs only 1.6% of the energy compared with Solution 1, and 6% of energy compared with Solution 2. This statement has been similarly stated in [7, 9]; however, no physical implantation and comparative validation are found in their efforts.

To evaluate the qualitative statement above, we built a sensing network using Waspmote 1, 2 and 3, each being set up with XBee modules and the wake-up hardware corresponding to Solution 1, 2 and 3. For each implemented solution, the mote was attached with a rechargeable 6600 mAh Lithium-ion battery. We programmed that when the Waspmote wakes up, MCU will measure the battery voltage level and calculate the current battery percentage.

A separate XBee coordinator was placed within the line-of-sight to each network of the Waspmote modules, forming a star XBee network in an indoor environment. To compare the difference in energy consumption between these three solutions, we minimized the possible power consumption from the front-end hardware, therefore no additional sensing units were used in this test. Each Waspmote was waked up by using its corresponding methods and joined in the XBee network every 4 hours.

Then they sent a ‘hello’ message to the coordinator which was always turned on. After that, each Waspmote read the current battery level, and then went back to its original state: XBee idle listening, IR receiver listening or RF receiver listening, respectively, as designed and implemented in Solution 1, 2, and 3. We monitored the test for about 130 hours for the three physical prototypes, and the battery levels were measured and recorded. The resulting energy consumption results are collectively shown in Figure 2.7.

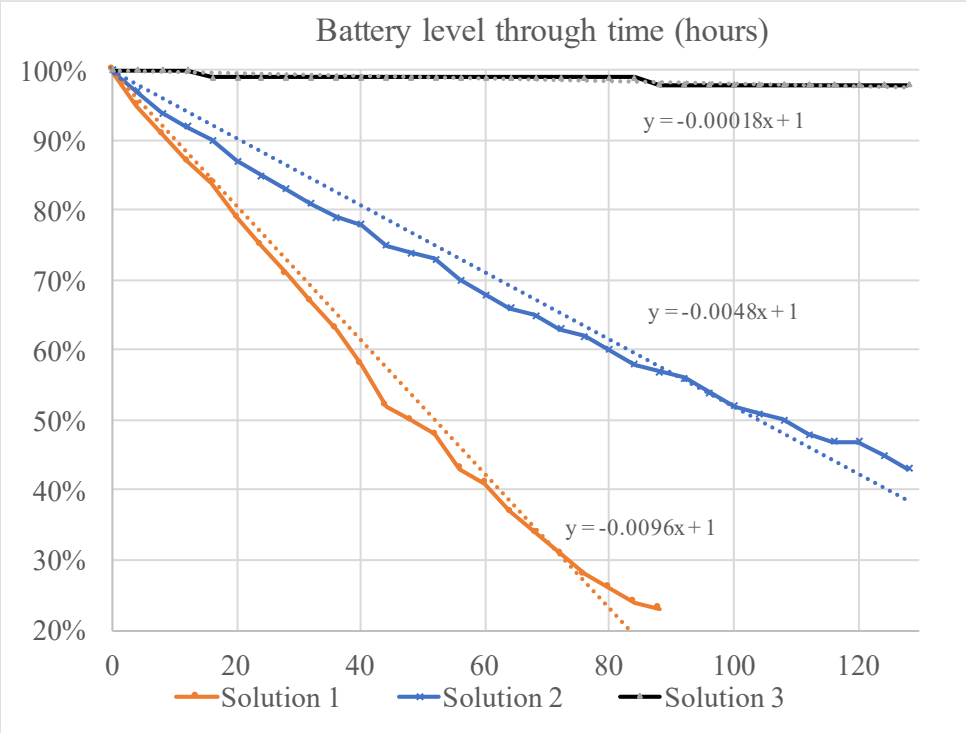

Figure 2.7 Experimental battery test and capacity dropping for the three different solutions

From the above results, we clearly see that Solution 1, in which the XBee module and MCU are always turned on, drains the battery out quickly in less than 90 hours. The data transmission in Solution 1 discontinued after 88 hours from the test since the battery level drops to 23%, and the Waspmote stopped working due to the

voltage is too low. In Solution 2, we can still see a linear drop in the battery level but with a slower rate than it is in Solution 1. As we stated above, most energy in Solution 2 is consumed by the IR receiver and the MCU, we can conclude that the XBee idle and listening states consume a large percentage of energy. Although we did not measure until the mote stopped working for Solution 2, we believe the battery level drop is linearly on a rate of 0.48% per hour and will last a total of about 208 hours (through linear fitting with a fixed intercept of 100%). Lastly, the battery level of Solution 3 did not drop significantly thanks to the RF wake-up solution. Due to the very low dropping rate, we only measured a 2% drop during the 130-hour test. Assuming a linear rate of consumption (through the linear fitting in Figure 2.7), we expect that the Solution 3 network would continue working for about 5556 hours (or an about 7.5-month period). This is a remarkable improvement compared with both Solution 1 and 2.

Last, if all the consumption rates are compared (as shown in the linear fitting in terms of the slope values), one can see that the power consumption rate from Solution 3 is about 3.8% of Solution 2, and 1.9% of Solution 1. This approximately confirms the analytical studies previously. In fact, we noted a better result (3.8% instead of 6%) from the analytical evaluation based on Figure 2.6, when comparing Solution 3 and 2. We believe this is attributed to that the actual XBee communication time is less than 1 min since there were not so much data being transferred in this test.

2.7 Conclusion

In this paper, we review the concept of aerial-ground wireless sensing network (AG-WSN) for its critical use in sensing in a remote and geospatially large or complex

space and particularly recognize the need of implementing such sensing solution in precision agriculture and structural health monitoring practice. We then recognize the technical challenge towards achieving energy efficiency in the ground sensors. Different wake-up mechanisms are then reviewed and compared. Among those mechanisms, we chose active radio frequency (RF) based wake-up method and implemented physically. The focus is on evaluating their performance to achieve energy efficiency on the battery-powered ground sensors. The following findings are achieved through the experimental evaluation in this work:

The experimental results in this paper indicate that the RF-based out-band wake-up mechanism can save a great deal of energy compared with the other two solutions (the infrared wake-up and the default duty-cycle methods). A direct comparison between the RF-based solution and the infrared-based solution indicates that the RF-based wake-up mechanism has noticeably better performance in the wake-up range, and has a tremendous improvement in the power consumption. Specifically, the results show that the RF-based wake-up mechanism can potentially save more than 98.4% of the energy that the traditional duty-cycle method would otherwise consume, and 96.8% if an infrared-receiver method is used.

The evaluation of wake-up time-delay by using a variety of different wake-up signal codes indicate that the time-delay is below 80 milliseconds; hence, the delay will not affect most opportunistic sensing applications (wherein the sensors sense the data at a time and transmit at a later time, then the sensors go back to the sleep mode until another abrupt event). Herein it is pointed out, however, that more strict time-delay

evaluation needs to be conducted if synchronization is critical between the sensors.

Given the two findings, it is concluded that the RF wake-up mechanism is the first candidate for implementing the proposed wireless aerial-ground sensing network for monitoring applications in large-scale geospatial or challenging spaces. The technical contribution also includes the use of a digital imaging approach to measuring the wake-up time-delay; and the resulting time-dependent rates of the battery-based power consumption using three different wake-up methods. This experimental and empirical knowledge may be extrapolated in similar sensing network research wherein sensor activation needs to be integrated.

The technical contribution also includes the use of a digital imaging approach to measuring the wake-up time-delay; and the resulting battery-based power consumption rates using three different wake-up methods. This experimental and empirical knowledge may be extrapolated in similar sensing network research wherein sensor wake-up needs to be integrated.

CHAPTER 3

EXPERIMENTAL INVESTIGATION OF AERIAL-GROUND NETWORK COMMUNICATION TOWARDS GEOSPATIALLY LARGE-SCALE STRUCTURAL HEALTH MONITORING

3.1 Introduction

The deficiency of civil infrastructure systems in the US has been recognized as a national challenge that, if not altered, would have a cascading impact on the nation's economy and competitiveness. For the stock of highway bridges in the USA, about 9.1% of them were structurally deficient in 2016 [95]. With the exposure to the unavoidable natural disasters, highly economical, rapid, and efficient structural condition and health assessment technologies are of critical importance for ensuring community resilience. To this end, periodic inspection is the mainstream method for managing most of the bridges and other civil infrastructure systems, which are time-consuming, laborious, and expensive. Innovative technologies for civil infrastructure data collection have been expected to transform this practice.

The state-of-the-art approach is structural health monitoring (SHM), which features the use of wired or wireless sensors, including the use of smart sensors in wireless sensing networks (WSNs) [14-17]. Most SHM technologies focus on sensing of vibrational data (e.g. dynamic acceleration, displacement or local strain data) due to external excitation, followed by signal processing and system identification methods for extraction of intrinsic system parameters (e.g. modal frequencies) and states (e.g. global and local damage proxies). In reality, however, for structures with slight to

moderate damage, such as local cracking and corrosion, visual or remote sensing based inspection is the most efficient approach to date. This is partially due to that in reality, local damage induced modal changes may be insignificant compared to changes due to environmental fluctuations (e.g. temperature and humidity) [96]. In contrast to SHM methodologies, remote sensing-based imaging technology provides a direct means for assessing structural damage. The underlying basis is that images of structures or structural components provide pixels that can be viewed as high-resolution 'sensors', which directly convey the appearance characteristics of structural condition. Among different remote sensing platforms, low-cost and highly mobile small Unmanned Arial Vehicles (UAVs or commonly called drones, such as quadcopters) are being treated as an emerging platform [18-20]. The use of such imaging UAVs has been proven effective in providing overhead imagery for civil infrastructure condition assessment, although operational challenges exist due to environmental factors.

It is noted that modern UAVs are often equipped with communication modules and can further carry sensing and routing payloads. This provides the technical feasibility of incorporating UAVs into a WSN that networks with regular ground-based sensors. On the other hand, the potential of integration UAVs into a WSN is also corroborated by a critical challenge in deploying practical WSNs in challenging environments. For instance, since sensors are usually battery-powered, field sensors are often deactivated and in the 'sleep' mode. Moreover, in a harsh environment or circumstance such as in disaster scenes where cellular networks are crippled, data may become ultimately inaccessible even if a local WSN survives. These challenges can be

overcome by taking advantage of the aerial mobility of the UAVs. One solution is to use a UAV to fly to the overhead of the ground WSN, and activate the sensors in an as-needed basis hence achieving maximum energy efficiency [26]. To access data from a ground WSN, the UAV may serve as a gateway to receive data from the ground sensors. It is noted that the concept of integrating UAVs into a WSN or realizing dynamic relay of communication has been similarly proposed by different researchers [27, 28]. However, no physical prototype or applications of such networks to civil infrastructure monitoring is found to date.

Recognizing the potential promise of integrating UAV-based imaging and ground-based WSN in improving the efficiency of collecting civil structures, the resulting network is termed *aerial-ground wireless sensing network* (AG-WSN) in this paper. In an AG-WSN sensing system, the UAV is adapted to achieve two immediate roles – as an imaging sensor providing overhead imagery and as a gateway (or data sink) that commands and receives data from the ground sensors. In an earlier effort of the authors [29], the concept of aerial-imaging and ground-sensing was proposed for use in the situation of disaster response in a geospatially wide area. In this paper, this concept is borrowed towards structural monitoring at a geospatial scale as well, wherein the health and conditions of a single large-scale structure or clustered structures (e.g. in a wide area such as a city block) are the concern. In recent years, it is noted that small UAVs are further investigated for the use in an interior or GPS-denied environment with the assistance of machine-vision based navigation [30, 31]. This implies that the proposed AG-WSN may be further extended into use in these challenging

environments.

Given such promise and towards deploying the proposed AG-WSN, however, one practical issue that remains not fully resolved is the interference between the UAV's and the WSN's operating frequencies. In practice, most UAVs use 2.4 GHz radio for flight control and 2.4 GHz Wi-Fi (802.11 g/n/ac) for imagery data feeds. For low-power sensing, ground-based WSNs often use the ZigBee (802.15.4) protocol, which may run at 2.4 GHz as well. In this paper, an AG-WSN prototype using commercial components is developed, and then the interference issue is experimentally explored.

This experimental paper contributes to the body of knowledge in terms of two empirical findings: (1) the key parameters affecting the short-range Wi-Fi and ZigBee interference and the experimental relations; and (2) the long-range optimal ZigBee transmission with the novel definition of the transmission comfort-zone and the sensitive parameter. Last, it is worth pointing out that the experimental methodology adopted in this paper is pragmatic towards deploying the proposed AG-WSN for the integrated monitoring civil structures at a geospatial scale. For analytically investigating the communication interference issue, rigorous anechoic-chamber studies are essential, which is often beyond the knowledge domain of civil structural and SHM engineers.

3.2 System Design and Potential Capabilities

In the proposed AG-WSN solution, the idea is to use a UAV as a remote sensing platform that feeds imagery data through the Wi-Fi link to the ground station; in the meantime, the UAV acts as a sink to gather data from ground-based sensing nodes

through the ZigBee communication. The ground-based sensor data can be of any modality including displacement, strain, temperature, moisture, and others that are pertinent to quantify and influence the health and integrity of the structures. The schematic design is illustrated in Figure 3.1. For a typical ZigBee network with a star topology, it incorporates two types of essential devices: one coordinator (as the gateway) and a number of end-devices (the sensing units). Accordingly, a minimal configuration is to integrate a ZigBee coordinator within the UAV that connects to another ZigBee enabled ground sensor.

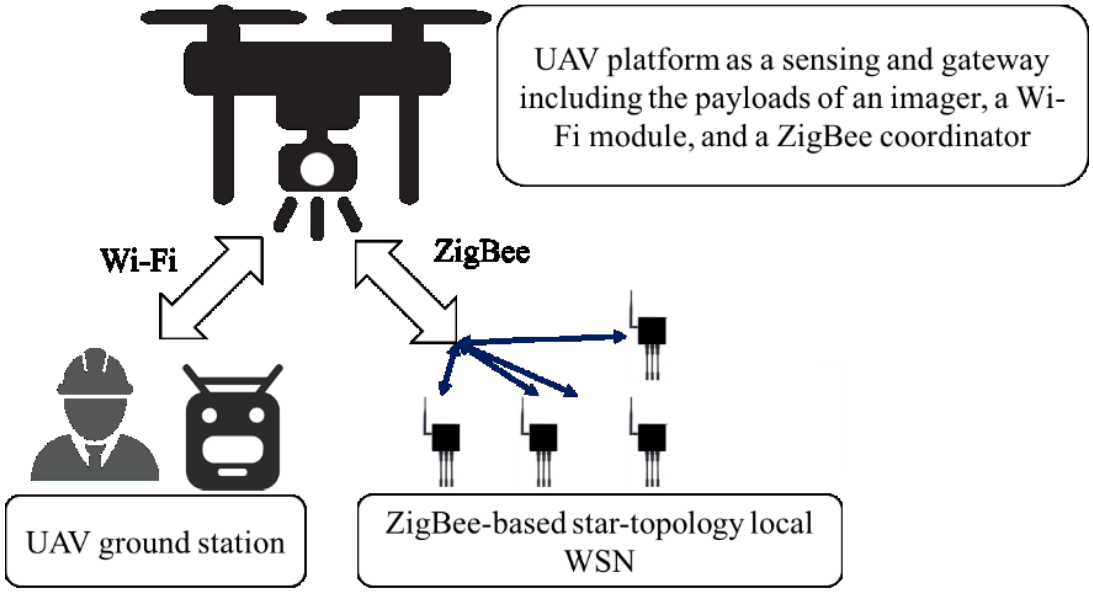

Figure 3.1 Illustration of the network topology for an AG-WSN with three system components: (1) UAV as a flying imaging and network gateway; (2) UAV ground station; and (3) a locally deployed Zigbee-based WSN (that may be part of the network installed on a civil structure).

With the configuration shown in Figure 3.1, it is noted that first, the UAV's two functions are not necessarily performed simultaneously. Nonetheless, to ensure the fly safety either with or without the visual line of sight (VLOS), video streaming through

the Wi-Fi link from the UAV to the ground station is critical and should be turned on continuously. As a result, the underlying communication-interference issue is outstanding once an AG-WSN is deployed in the field, which is the challenge to resolve in this paper. With the basic sensing functions of the AG-WSN, three other potential capabilities and opportunities of an AG-WSN network are envisioned and summarized as follows.

1. The imaging (including laser-based scanning) payload at the UAV in an AG-WSN can be used to measure structural displacement remotely through photogrammetric processing and mathematical optimization. This promise has been showcased in several recent endeavors with experimental verification in a laboratory or ideal environment [97-99], which provide a great promise in overcoming the cost of deploying contact-based sensors to civil structures in a challenging environment. However, it is recognized that, first, even considering such logistic challenges, contact-based sensors are yet essential when obtaining in-situ environmental measurements (e.g. temperature and moisture etc.) and the ground-truth structural measurements. In addition, it is asserted that other significant challenges exist towards direct UAV-imaging based structural monitoring, such as wind-induced aerodynamic disturbance and difficulty in achieving UAV-motion invariant estimates [97].
2. The proposed AG-WSN framework provides the next-generation

solution to embedded computing towards the real-time delivery of structural health analytics. First, although the state-of-the-art wireless sensors today are equipped with basic onboard or embedded processing capability, e.g. as found in the sensor boards of Xnode, Imote2, and WaspMote etc. described in [100], mostly the computing is limited to simple preprocessing due to computing speed and power consumption. On the other hand, modern UAVs are usually equipped with a much more powerful embedded computer (e.g. one used in our research is powered by a Xilinx SoC that is powered by a dual-core ARM processor and an FPGA processer) and higher-capacity lithium-ion polymer batteries, which can be exploited to realize the notion of realistic edge-computing towards online system identification and damage-scene understanding [101].

3. As shown in Figure 3.1, the locally deployed WSN on the civil structures implies that the WSN may be a sub-network of the WSN system for the monitored structure. This further signifies that the flying UAV can serve both as an in-situ server in receiving and processing the ground data and a 'head' sensor node for the sub-network in the ground. Through flying to the next or adjacent sub-network deployed to the structure, this operational modality provides an unprecedented opportunity for implementing the well-explored decentralized SHM for a large-scale structure [14, 102, 103], although significant research challenges are to

be recognized; and some envisioned arguments are provided later in this paper.

3.3 Technical Background in Wi-FI and ZigBee Interference

For the operating frequencies of Wi-Fi and ZigBee, besides several optional frequency bands (e.g. 868 or 915 MHz for wireless personal area network or WPAN; and 6 or 60 GHz for wireless local area network or Wi-Fi), industrial Wi-Fi devices generally use the 2.4 GHz frequency band, which overlaps with the most widely used 2.4 GHz for ZigBee devices. With this sharing of the same frequency band, first of all, numerous efforts have indicated the presence of ZigBee and Wi-Fi interference in a close range [104-108]. Second, the fact that small UAVs (e.g. a quadcopter) are size-sensitive to the addition of flight payloads renders the possible close-range interference more significant. In the meantime, interference will always trigger higher power consumption and shorten the aerial endurance besides risking the UAV flight control. Therefore, an investigation of how Wi-Fi interferes with the low-power ZigBee communication in a UAV platform is practically needed.

Some researchers attempt to find ways to avoid or resolve the interference when both networks are deployed. Huang et al. (2010) argued that there exist abundant opportunities for ZigBee and Wi-Fi to coexist in the same or overlapping channels [105]. They developed a frame protocol to achieve the trade-off between the throughput and the packet delivery ratio (PDR). Zhang and Shin (2011) used a frequency flip scheme to avoid this frequency overlap, in which a ZigBee node is deployed to notify a nearby Wi-Fi network to prevent mutual interference between the two [108]. A similar

idea was reported by using a hybrid device to coordinate messages between the Wi-Fi and the ZigBee networks [104]. In addition, the work of Xu et al. (2011) developed a scheme that detects a Wi-Fi network and then automatically changes the ZigBee channel to avoid interference [107]. Other researchers found that due to the low power requirement, ZigBee packets are easily corrupted by strong Wi-Fi interference. As such, one potential solution is to modify the ZigBee packet to potentially reduce the interference. For instances, Liang et al. (2010) used multi-headers in ZigBee packets that provide header redundancy to increase PDR and claimed that in most cases, the ZigBee packet header is the only corrupt zone of the whole packet under the Wi-Fi interference [106].

There are a few endeavors that aim to evaluate the ZigBee network performance under Wi-Fi interference through numerical simulation and experimental verification. Theoretical modeling of ZigBee interference in terms of packet error rate (PER) under Wi-Fi and Bluetooth was reported [109]. In Yi et al. (2011), the authors adopted this theoretical model and further verified the simulation by physical testing that the distance between the Wi-Fi and ZigBee devices and the offset of the center-operating frequency between the two are the two major factors that affect the ZigBee performance [110]. They reported that a distance of two meters in most cases would be safe if there is an offset frequency of 8 MHz between the ZigBee and the Wi-Fi. This is a notable finding for deploying ZigBee and Wi-Fi networks using commercial products without considering the aforementioned frequency-based adjustment or packet modification schemes. However, for considering deployment of a UAV-based network, it is hard to

achieve the aforementioned configuration since most commercially available quadcopter UAVs usually have a form factor less than 2 meters. Another interesting white paper shows that different ZigBee devices using different chipsets have quite unique results under the impact of Wi-Fi [111]; hence, technically the shorter distance may exist. Unfortunately, most commercial ZigBee devices and chipsets including the ones used in this paper are not in the test results in Thonet et al. (2008). Last, it is pointed out that although there are analytical models (with numerical evaluation) for ZigBee interference with Wi-Fi [109, 110], field-based testing is the ultimate approach. This physical experimentation approach is adopted in this case study.

3.4 Experimental Evaluation

3.4.1 System Prototyping and Testing Environment

As shown in Figure 3.2, an AG-WSN prototype is developed based on a commercial drone (DJI Phantom 3 Professional) that carries an imaging camera with the real-time Wi-Fi data link to the ground station. Two Waspmote® sensor boards from Libelium are used (each with an XBee-based ZigBee communication module made by Digi with the Silicon Labs EM357 SoC transceiver chipset operating at 2.4GHz) are used to construct a minimum (two-node) ZigBee network. The native Wi-Fi antenna of the UAV for video transmission is built into the front-left landing gear. The insert picture in Figure 3.2 shows the Waspmote board that is attached to the UAV. The other (identical) Waspmote board is placed at the ground as the end-device.

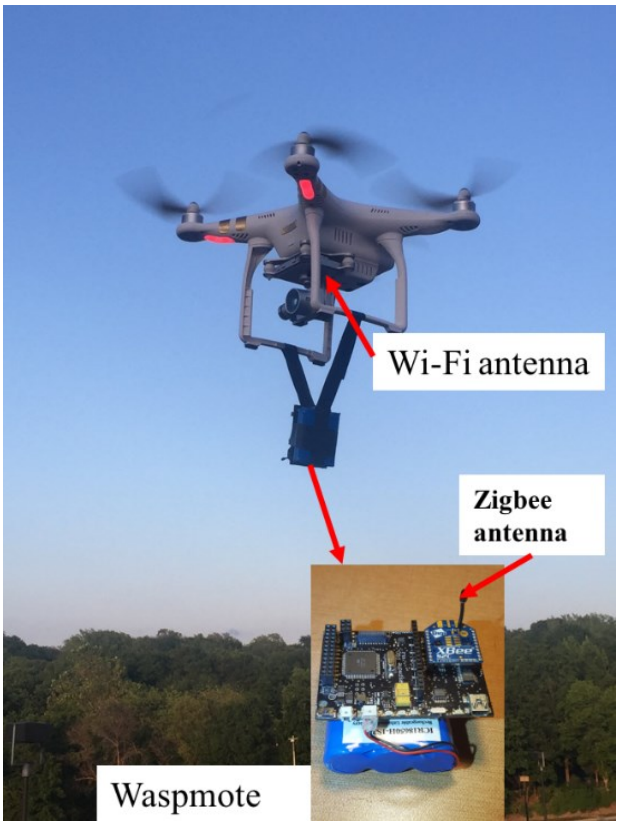

Figure 3.2 Physical prototype of the UAV system with a minimum AG-WSN configuration: one commercial UAV with a set of payloads including an imaging camera with a Wi-Fi link to the ground station, and two ZigBee devices (one as the UAV payload and the other at the ground level).

It is noted that the electromagnetic radiation is primarily determined by the antenna gain, and hence the data transmission between the antennas of two end devices. Qualitatively, if one reduces the Wi-Fi antenna gain (reducing the power need by the Wi-Fi module as well), the ZigBee will definitely have better performance on both range and the PDR. However, this may impact the quality and range of the UAV's video-streaming feedback. On the other hand, if the ZigBee's antenna gain is increased (hence entailing higher voltage of power supply), the performance in terms of both PDRs and ranges will be improved under the Wi-Fi interference. When realizing the prototype as shown in Figure 3.2, commercial products were utilized, which provide no possibility of changing the gain by programming. In this experimental study, the

antenna of the DJI UAV has a gain of 2.82 dBi , which is relatively strong to accommodate its video transmission function in the visual line-of-sight distance in the outdoor environment; whereas the PCB antenna on the XBee board has a low gain of 0.6 dBi considering that its primary use is for constructing a local sensing network. Without changing the gains, this fixed gain difference implies that the ZigBee communication will be heavily interference by the Wi-Fi signals.

The experimental site for the long-range testing is a public place with minimal possible environmental radio interference. At this site, no Wi-Fi signals were found along the UAV flying path, and the only possible effects may come from cellular networks. Rigorous experiments may be done in a controlled environment (e.g. large-scale anechoic chambers) to achieve data for validating analytical models. Nonetheless, this work adds value in a way that all the data and observations are achieved in a real environment that mocks many urban or remote environments; towards providing the most realistic guidance for practical system implementation, the experimental framework and findings are considered an addition to the knowledge body.

3.4.2 Experimental Design

Using the prototype setup in Figure 3.2, it is noted that the Waspmote® sensing devices (one acts the coordinator, and one as the end-device) are actually two identical sensor boards both with the XBee communication modules, which are hence interchangeable in terms of serving as the coordinator or the end-device role. Therefore, for the practical evaluation purpose, the component of the XBee module at the ground level can be connected to a computer laptop to act as the coordinator. This reverse

configuration is convenient since the XBee-laptop platform can readily run the developed testing program to conduct the evaluation. To ensure the likely interference minimized at the ground, a 10-meter distance is kept between the ZigBee coordinator and the UAV's base station. With the prototype system in the air shown in Figure 3.2, Figure 3.3 illustrates the primary configuration and the geometric variables for the interference evaluation: D – the distance between the UAV and the laptop; d – the distance between the Wi-Fi and ZigBee (XBee) antennas; and θ – the relative angle between the two antennas in the UAV configuration space.

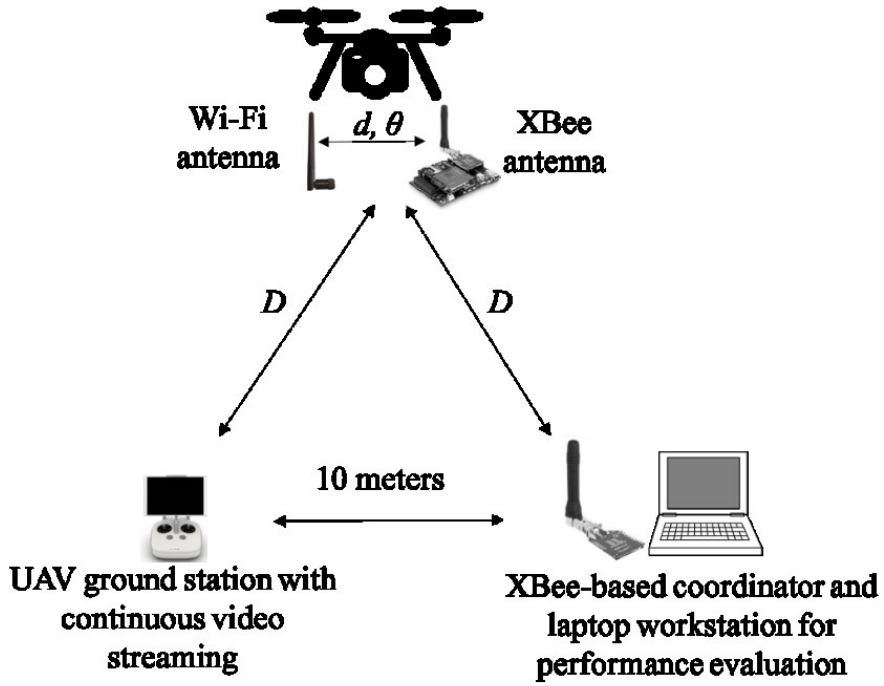

Figure 3.3. Illustration of the experimental setup and the configuration variables.

To minimize other possible factors that may affect the test result, the Wi-Fi center frequency was set precisely at 2486 MHz and ZigBee center frequency at 2455 MHz according to Yi et al. (2011), which states that the larger frequency offset between these two, the less interference is likely to occur when the distance between Wi-Fi and

ZigBee stays the same. Second, the power of the Wi-Fi and the ZigBee modules are both set as a fixed value. During the testing, the UAV maintains communication with the ground station using the Wi-Fi channel and sends the video feed to the station. The ZigBee coordinator at the ground is controlled to send packets of 50 bytes repeatedly to the end-device attached to the UAV (both the coordinator and the end-device have the same XBee antennas). The end-device then returns the received data back to the coordinator. By monitoring the number of packets that travel back to the coordinator, the PDR (Packet Delivery Ratio) is defined and measured:

$$\text{PDR} = \frac{\text{Number of packets Returned}}{\text{Total number of packets sent out}} \times 100\%$$

In the following tests, a total of 1000 packets are sent to calculate the PDR at a prescribed condition.

3.4.3 Test-1: Interference at Short-range Communication

In an initial test with no Wi-Fi interference (where the UAV was turned off without video feeding and the UAV is moved away from the Zigbee coordinator), the ZigBee coordinator and the ZigBee end-device was found to be able to communicate at a 99.6% PDR at 800 meters (which is the maximum the line-of-sight distance considered in this paper). When the Wi-Fi was turned on (UAV was turned on, and the standard video, 720p/6000kbps/30fps, is feeding to the base station), it was found that the interference became dramatic with the PDR less than 50%. To observe the effects of the relative positions of the Wi-Fi and the ZigBee antennas, the set up shown in Figure 3.3 was used, in which the UAV and the ZigBee coordinator distance (shown as *D* in Figure 3.3) was set 5 meters, while the UAV was set hovering with the Wi-Fi video

feeding set on. With this configuration, two tests were conducted: first, the Wi-Fi and the ZigBee antennas were set orthogonal to each other ($\theta = 90^{o}$), then the PDRs were evaluated at eight different distances between the two antennas ($d = 2$, 3, 4, 6, 8, 10, 15 and 20 cm); and second, the antennas were set parallel to each other ($\theta = 0^{o}$), the PDRs were obtained at the same distance values. Figure 3.4 shows the test results of the PDRs as the relative antenna positions change. The *x*-axis shows the distance in centimeters between the UAV's Wi-Fi antenna and the end-device's ZigBee antenna, and the *y*-axis marks the evaluated PDRs in terms of percentage.

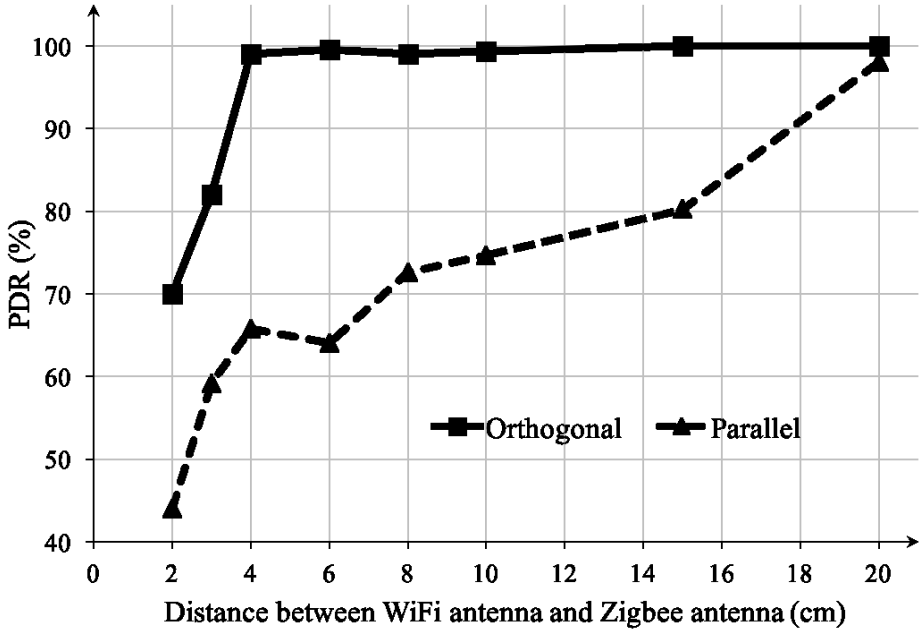

Figure 3.4 Plots of PDRs in relation to the Wi-Fi and ZigBee antenna distances (at two relative angles: orthogonal and parallel).

First of all, the results reveal that even at a short-range range of 5 meters, if the Wi-Fi antenna is too close to the ZigBee module antenna, the ZigBee communication was found to bear heavy interference. When *d* is at the extreme close range (2 cm) and at a parallel position, the ZigBee PDR is about 45%. As the distance *d* increases, the

PDR increases, and at about d = 20 cm, the PDR reaches approximately 100%, indicating no interference.

During this short-range test, it is also noticed that that the interference is much greater when the two antennas are parallel than when they are at the orthogonal position given the same distance between the two antennas. At the orthogonal position, when d = 4 cm, the interference is approximatively negligible; whereas for the case of being parallel, the PDR increases much slowly at d increases. From the d = 4 to 15 cm, the parallel position provides about 20% to 35% less in measured PDRs than the orthogonal position does.

Additional relative positions at different angles were tested by fixing the distance between the ZigBee and Wi-Fi antennas at 4 cm. In Figure 3.5, more relative angles ranging from 0° (parallel) towards 90° (orthogonal) are shown as consistently increasing with the PDRs. Combining the observations in Figure 3.4 and Figure 3.5, and considering the relatively small configuration space within a UAV (e.g. only a relative distance less than 50-cm is allowed), an orthogonal position between the UAV's Wi-Fi antenna and the ZigBee antenna should be preferred.

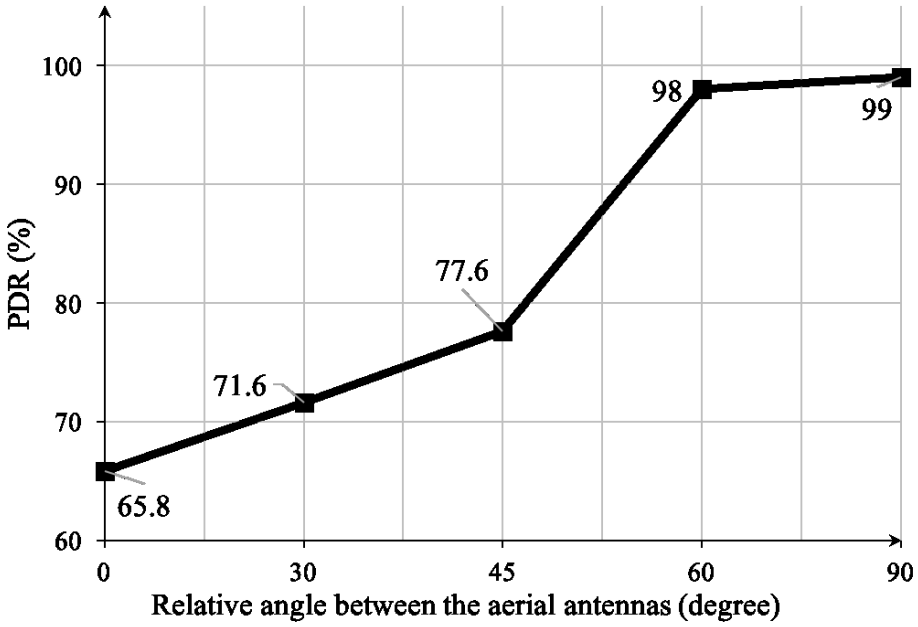

Figure 3.5 Plot of PDRs in relation with the antenna angles (at a fixed distance d = 4 cm).

3.4.4 Test-2: Interference in Long-range Communication

Two flight tests were conducted to evaluate the long-range Wi-Fi interference. To minimize the short-range interference between the Wi-Fi and the ZigBee antennas, the two antennas were placed far more apart than 20 cm and in an orthogonal position (according to the results from Test 1). Therefore, the interference if any is the result of a long-range interference between the Wi-Fi and ZigBee signals. In this test, two different distances between the two antennas were adopted: d = 30 cm, and d = 50 cm. Then the ZigBee coordinator and the UAV controller were fixed 10-meter apart and the UAV was controlled to fly away from this position at a height of 15 meters above the ground. At each position of the UAV (D = 10, 20 50, 75, 100, 150, 300, 450, 600, and 750 meters; all ground distances were measured through the GPS readings from the UAV control station), the UAV was carefully yawned such that the ZigBee antenna of

the end device in the UAV is parallel with the ZigBee coordinator's antenna to keep maximum signal strength. At each distance, the UAV hovered until one PDR test was done. The test is done over a flat field that is approximately 60 meters wide and 800 meters long. Figure 3.6 illustrates the test field and the flight path.

Figure 3.6 Flight field and path for the long-range interference test (courtesy of Google Map).

Figure 3.7 shows that when the distance *d* between the UAV's Wi-Fi and ZigBee antenna is 30 cm, the ZigBee communication can overcome the Wi-Fi interference (with a PDR close to 100%) as long as the communication distance (between the coordinator at the ground and the end-device in the air) is within 50 meters. When *d* increases to 50 cm, the distance of 100 meters is a greater threshold for the ZigBee communication to overcome the Wi-Fi interference. In this paper, this threshold for achieving negligible interference is defined as a ZigBee communication 'comfort zone' for UAV-based long-range mixed Wi-Fi and ZigBee data transmission.

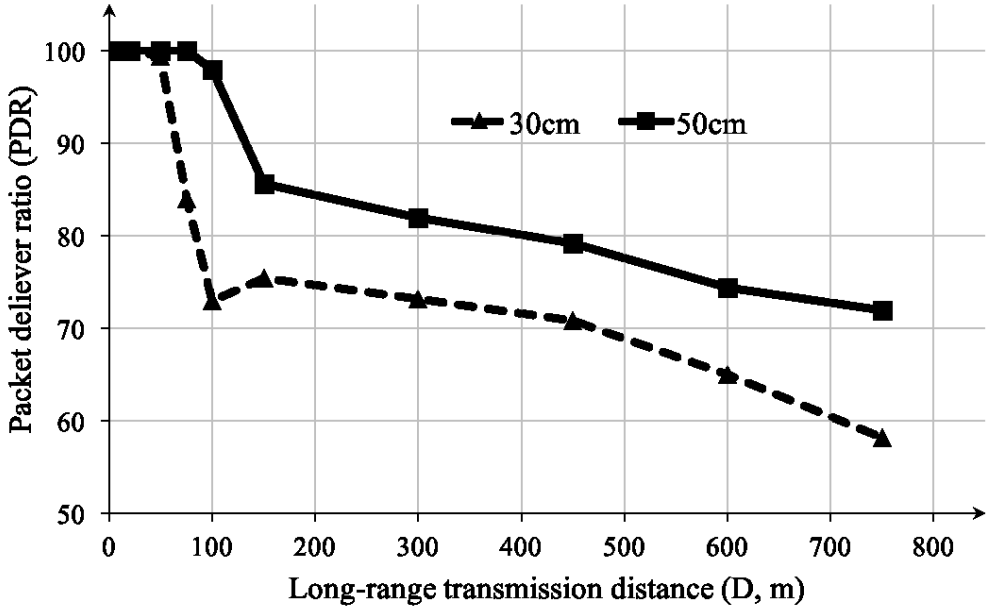

Figure 3.7 Plots of long-range PDRs in relation to the transmission distance between the ZigBee devices.

It is observed from Figure 3.7 that the ZigBee PDRs at both flight tests quickly drop when the range is out of the comfort zone. After a certain distance (D = 150 meters), the PDR drops more slowly; approximately, the rates of dropping (the slopes) are about the same at the two antenna-to-antenna distances (d = 30 cm and 50 cm). One speculation is that when the distance of the two ZigBee modules exceeds a certain range, the Wi-Fi interference becomes less significant and the PDR dropping is more of an attenuation function of distance. However, this may need further experimental evaluation. In this paper, the main concern is to find out the condition at which the Zigbee communication can survive the Wi-Fi interference or operate in the comfort zone.

Figure 3.7 implies that the larger the value of d, the larger a comfort zone one may obtain. However, the sizes of most small commercial UAVs in the market

physically limit a too large distance between the antennas. Thus, it is meaningful to find an envelope that describes the relationship between the Wi-Fi/ZigBee antenna distance d and the range of the comfort zone. To determine the envelope of the comfort zone, with the same long-range testing configuration as used above, different antenna distance values (d varies from 20 to 80 cm, and θ remains 90º) were tested. At each of the distance values, the communication range (D) was determined at which the PDR was above 99.8% (namely treated as the maximum range of the comfort zone). With this testing, the envelope of the comfort zone is defined, and Figure 3.8 summarizes the observed values.

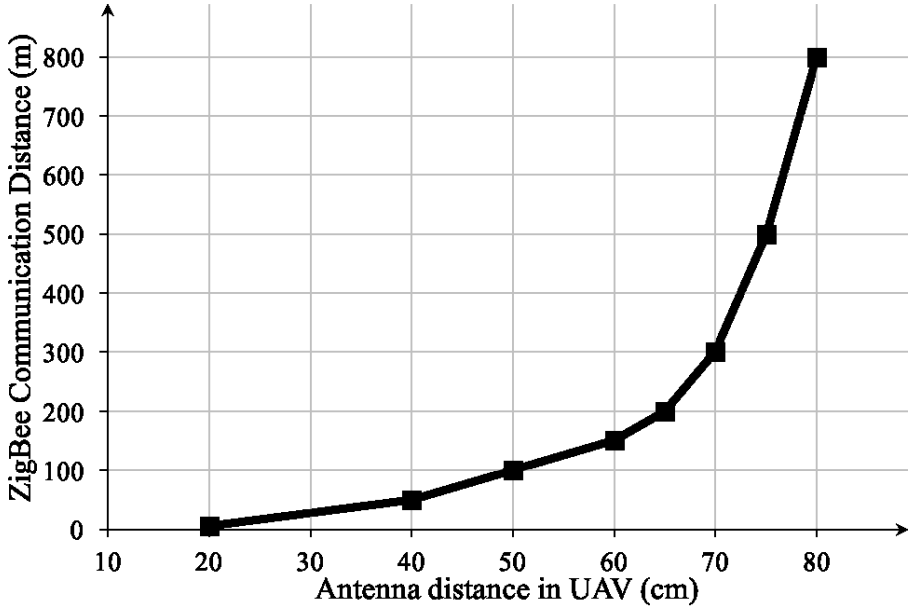

Figure 3.8 Comfort zone envelope as a relation between the ZigBee communication distance and the antenna distance in UAV.

From Figure 3.8, one can safely conclude that a few centimeters of increment in d can lead to a very significant gain in enlarging the comfort zone. It is stated that

this result is not found in the literature, which can assist the implementation of the proposed AG-WSN, especially when a commercial UAV is considered that comes with a small form-factor and limitation for adding payloads.

3.5 Discussion

Towards deploying the proposed AG-WSN network to large-scale structures or structure clusters, there exist several major challenges. These challenges are described as follows and the solutions that may partially resolve these challenges are suggested as well.

Environmental and operational challenges. This category of challenges includes the operation of UAVs (especially the multi-rotor copters) during a vehement weather condition (e.g. heavy raining, high-wind, and very low-visibility days). If the camera is used to measure structural displacement, as indicated in [97, 98], these challenges are not fully resolved to this end. For instance, the wind-induced aerodynamic disturbance to the UAV will violate the 'small-rotation' assumption for the UAV towards extracting the true structural displacement from the images. Even with a benign weather condition, the UAV in the field may often fly out of the plane when imaging the structure that violates the in-plane motion assumption. With these challenges that are present to date, contact-based wireless sensors are still poised to be the most reliable solution to this end, which further ratifies the value of the proposed UAV-based AG-WSN solution. As it is pointed out previously that since the primary goal of flying the UAV in our proposed solution is not to employ the imaging payload to 'measure' structural

displacement, moderate weather conditions should be acceptable if the UAV is capable of flying from an operational safety point of view, as long as the data links are operational between the UAV and the ground sensors. Another operational challenge is automatic obstacle avoidance when deploying the UAV over a complex space (e.g. in a dense urban environment). If the UAV flies too close to the structures, amid the complex aerodynamic effect (similar to the near-ground effect for any plane when landing) the UAV needs to be equipped with an automatic obstacle-avoidance capability using a vision or radar-based approach [112, 113].

Energy optimization challenge. When performing monitoring over a geospatial wide-area with multiple structures and numerous local sensor networks, the UAV needs to fly over these structures or sensors of interest. Given the limitation of battery technology to date, the UAV needs to fly to all locations with an optimal path that minimizes the energy cost. Theoretically, this belongs to the traditional traveling salesman problem (TSP). With the experimental efforts and findings in this paper, particularly the recognition of the 'conform-zone' radius when transmitting data in a long distance, the resulting problem becomes a traveling salesman with neighborhood problem (TSNP), and several analytical solutions can be found in [114, 115].

Optimized sub-structuring for sensor placement (or sub-networking topology), and the development of decentralized sensing and computing. As described previously, the proposed AG-WSN provides an unprecedented opportunity of implementing a SHM solution based on decentralized sensing, wherein the UAV serves as a dynamic 'head sensor' for a local sub-network and a real-time 'edge-computing' server. However,

several research challenges can be recognized. It first challenges the validity of the existing decentralized system-identification algorithms (e.g. the random decrement method in [102]), considering the great flexibility due to the 'flying' mechanism of the UAV. Second, the network topology is not geospatially static but dynamic due to the airborne flexibility of the UAV as the mobile gateway, which belongs to the arena of opportunistic routing; and several UAV-based solutions are explored in the literature [116-118]. The aforementioned energy optimization additionally imparts more constraints to the problem.

3.6 Conclusion and future work

In this paper, starting with the motivation of developing a UAV-based aerial-ground WSN for realizing integrated remote sensing and structural health monitoring, the potential interference issue between Wi-Fi and ZigBee communication is experimentally investigated. By developing a prototype system with the commercial components, this case-study paper determines the key factors that affect short-range interference and the long-range data transmission performance. It is observed that the relative position of the Wi-Fi and ZigBee antennas and the distance between them are the two major factors that impact the communication. In the long-range experiment, the ZigBee data transmission is tested as the range varies up to 800 meters (the line-of-sight distance). Defining the range with the packet delivery rate of 99.8% as the ZigBee 'comfort zone', the effect of the ZigBee/Wi-Fi antenna distance is further determined and recognized as a sensitive parameter. It is found that with a few centimeters of increment in this distance, the comfort zone range can be improved significantly.

It is worth mentioning that this test result is based on the specific UAV and ZigBee modules that are commercially acquired. Nonetheless, the experimentation framework should be applicable to other commercial products, and similar relations as reported in this study should be expected. Moreover, the findings in this paper provide the guideline in designing the mixed communication configuration in deploying the proposed aerial-ground sensing network wherein Wi-Fi and ZigBee networking are both involved, especially when the ranges of operating frequencies at both overlap.

Two important parameters that may impact the Zigbee PDR, the Wi-Fi video feed quality and the power level for both Wi-Fi and Zigbee radio, need to be further investigated in the future. In the current experimental setup, the video feed quality is not changeable, nor the power level. On the other hand, Zigbee communication may indeed impact the UAV Wi-Fi/video feed quality, which can be another research focus using the setup that comes with adjustable video-streaming quality and power levels in the UAV.

It is noted that in this effort that focuses on defining the concept of the aerial-ground wireless sensing and investigating the network interference within such a novel network, realistic structural response and environmental data are not analyzed. The future efforts based on finding in this paper include the development of heterogeneous sensing including low-speed environmental sensing (e.g. temperature and moisture data at a rate of one data point per minute) and fast structural sensing (e.g. acceleration data at a rate of 200 points per second), and the aerial real-time data acquisition and computing. The subsequent investigation will include the implementation of a

decentralized sensing solution that is optimized for either a single large-scale structure or a geospatially-large structure clusters in an urban area. The implementation task further includes the edge-computing based data processing and system identification towards fully real-time flying, sensing, and delivering of structural health and condition assessment analytics.

CHAPTER 4

SPATIAL PATH-ENERGY OPTIMIZATION FOR TACTIC UNMANNED AERIAL VEHICLES OPERATION IN ARIAL-GROUND NETWORKING

4.1 Introduction

With advances in autonomous navigation, positioning, mechatronics, and in general robotics technologies, small to miniature-sized unmanned aerial vehicles (UAVs; or colloquially called drones) are becoming much low-cost, agile and effective, hence witnessing their ever-increasing use in many social / economic sectors. Today's professional UAVs are usually equipped with the latest GPS technology; and many small UAVs, especially the multi-motor ones can fly following the predetermined GPS waypoints. Some advanced drones possess small form-factor radar or vision sensors that enable its sense-and-avoid capability [45-47], and therefore fly beyond (visual) line-of-sight (BVLOS or BLOS).

On the other hand, particularly for the multi-rotor UAVs which can take off vertically and fly at a hovering mode, waypoint-based flight control is not critical. As a matter of fact, flying over many pre-determined or locations opportunistically or as demanded in the real-time becomes a very attractive feature. Three examples are illustrated herein. First, one of the most popular use of UAVs is to provide visual monitoring or surveillance data through its camera payload, from which 2-dimesnioanl (2D) or even 3D mapping products can be rapidly obtained. This capability is found useful and effective in many arenas in the architecture, engineering, and construction (ACE) industries, precision agriculture, environmental monitoring, disaster and

emergency response. Given a geospatially large field or a 3-dimensionally complex built object (e.g. a high-rise building or a long-span bridge), the UAV can fly to predetermined or opportunistically encountered locations. The second application setting is an emerging technology trend is UAV-based delivery, for which technology giants such as Amazon and Google are competing to take the lead. It is expected by many that UAVs-based delivery would be a key link in the modern logistics transportation system. If this happens, it is obvious that in a typical route, the UAV many carry multiple packages to deliver at a number of locations (or the opposite, the UAV picks up packages at a number of locations). Considering the limited power of a UAV, which is usually battery-powered, it is obvious that the UAV should optimally travel to these different locations with the shortest distance (hence less flying time further less energy consumption). This is an alternative expression of the classical traveling salesman problem (TSP). Several existing efforts are found that utilized a TSP based optimization framework to optimizing UAV's spatial path [38, 119-123].

In this endeavor, the authors recognize a novel application of UAVs that the UAVs can be used as aerial gateways to connect with ground-based wireless sensing network (WSN). This application, still its infancy or conceptual stage, can be considerably useful for several application scenarios, where ground-based sensing and aerial remote sensing are both relevant, such as for agriculture wherein ground-truth soil/crop data can be used to validate or fuse with the remote sensing data. In this effort, the application setting is structural health monitoring (SHM) and condition assessment at a large geospatial scale for civil structures and life-line infrastructure systems that

often are massive and spatially complex (e.g. urban buildings, long-span bridge, and power transmission lines/towers, etc.). In addition, we have proposed and developed a prototype of realizing a wireless aerial-imaging and ground-sensing network; or in short, aerial-ground wireless sensing network (AG-WSN) [48] for its possible use in geospatial-scale SHM and condition assessment.

For civil structures that are critical to the society, sensors and especially WSNs can be installed for these structures in their lifetime hence achieving 'smart structures'. The continuous health monitoring through these WSNs provides stakeholders a basis for ensuring public safety and a ground for decision-making when dealing with unexpected damage or losses [2]. As shown in Figure 4.1 (a), the traditional approach has been collect the response of structures due to environmental or hazards-induced vibrations through the wireless sensors then a process of system identification is typically entailed to extract the possible change of structural integrity or damage [14-17]. In reality, however, for structures with slight to moderate damage, such as local cracking and corrosion, visual or remote sensing based inspection is the most efficient approach to date. However, in practice, there is no need to constantly monitor the structures, as most damage develop slowly due to material aging or environmental deterioration. This implies that two possibilities. First, the ground sensors for the SHM over different structures can be deactivated (in sleep mode); then activated when needed to save energy, and the UAV can serve as the 'activator' and then becomes a data sink to collect the data. This would work for critical structures that are installed with WSN already. Second, for the majority of the structures which are not installed with sensors,

the UAV can fly and deploy sensors (acting as a delivery robot) and then construct a WSN in the meantime to collect data a data sink. In either these two scenarios, the UAV can function it does typical to perform remote imaging and inspection of the civil structures that it visits. For this function, many efforts have explored its use [18-20]. This further corroborates the necessity of combining WSNs and UAV-based remote sensing technologies.

(a)

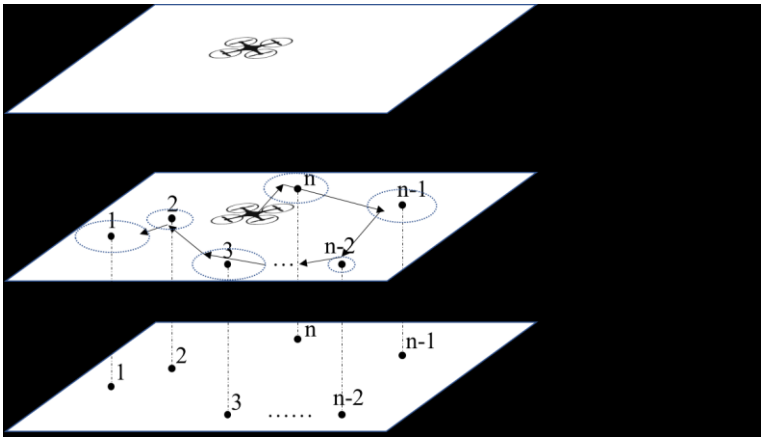

(b)

Figure 4.1 Proposed AG-WSN. (a) Conceptual illustrations of the proposed aerial-ground sensing network (AG-WSN) for structural health monitoring and condition assessment; and (b) idealization by collapsing the three-dimensional (3D) flight over the sensors into 2D plane, where each sensor has a communication range (for any sensor herein, the range forms a local region). The UAV can fulfill the data collection task for a sensor if it enters its local region

Given the aforementioned description of the AG-WSN concept for geospatially large-scale SHM and condition assessment, one may recognize that the primary energy constraint for the UAV does not vanish as it is described for the UAV-based parcel delivery or pickup context. Nonetheless, in this effort, it is further identified that the problem is not a typical TSP problem towards minimizing the energy cost, in which the travel aims to precisely reach isolated points (at the sensor nodes). The primary difference is that the UAV is not necessary to fly exactly to the 'node' point of the ground sensor in order to collect data; instead, as long as it reaches a communication range despite the possible packet loss in communication, the task of data collection can be completed. Assuming that the sensors are in one plane and the UAV flies in a parallel plane, either the spatial topology of the sensors or the UAV and its flight paths can be projected onto one unified plane (a virtual configuration plane). As illustrated in Figure 4.1(b), this implies that the UAV needs to find the paths to visit the communication ranges (i.e. neighborhoods) of the individual sensor nodes once and collect data from all nodes with the minimal energy cost. This problem is a generalization of TSB, and is essentially the Traveling Salesman Problem with Neighborhoods (TSPN).

With this proposition, this paper formulates the TSPN problem in the context of spatial path-energy optimization for a UAV-based AG-WSN system. Through exploiting a non-convex mixed-integer nonlinear programming (MINLP) framework, this paper concerns three novel and related contributions. First, when constructing the objective function, a new communication range function with package loss is considered. Second, when defining the objective path-energy function, both the energy

cost due to the forward-moving and hovering modes are both incorporated. Third, when defining the neighbor radius (physically the distance from the UAV to a sensor node), a novel classification of the solutions is proposed, including two solution bounds and one fully dynamical path-energy approach. These formulations and propositions are not found in the literature. Nonetheless, the problem at hand in this paper is not a standard TSPN.

This Chapter is organized as follows: Section 2, first a short review of related work is provided, and then the TSPN problem in the context of the proposed AG-WSN is described. Section 3 provides the mathematical formulation including the consideration of the UAV flight modes (forward-moving and hovering), and the mixed-integer nonlinear programming is described, and the solution classification is proposed. Subsequently in Section 4, multiple simulation results are given to evaluate the performance of the numerical optimization procedure. Section 5 provides conclusions and further remark on the possible improvement and research in the future.

4.2 Related Work and Traveling-salesman Problem with Neighborhood

4.2.1 Related Work

The most traditional and reliable way for wireless sensing network (WSN) method to collect sensing data is using a stationary gateway with multi-hop routing [32]. In some conditions, however, it is not possible nor efficient to use such topology due to the environmental and energy restriction. The alternative method is to deploy a mobile robot as a network gateway to collect data from the sensor nodes either in the multi-hop routing [33, 34] or the star topology [35-37]. Mobile robots including ground

robots and UAVs as previously described can either move or fly following GPS-enabled waypoints or approach to tactically selected locations, hence perfectly serving as a rely node of a gateway for the ground sensor networks.

Numerous efforts are found in which the TSP or TSPN frameworks were employed for mobile robotic path planning within a wireless sensing network, which are in a way similar to the UAV's gateway role in an AG-WSN. The authors in [36] proposed to use multiple ground robots to gather data from one sensor network, for which it was termed a 'k-TSP' problem. In this topology, the gateway remains stationary while the robots act as relays for the sensor nodes. Therefore, their implementation of such routing mechanism is limited to a TSP not actually a TSPN. A different approach was conducted in Wei et al. (2012) [37], where the routing mechanism aimed to guarantee that a robot can always return to the docking station rather than to provide a global optimal solution. Yuan et al. (2007) reduced the computational time of solving TSPN by constructing a TSP tour first and then apply the Evolutionary Algorithms to achieve the search space reduction [42]. Last, a survey of mobile sink routing for wireless sensor networks is found in the literature [124]. However, most work are related to wireless network routing and heavily rely on data relaying of multiple sensor nodes. To the author's knowledge, no TSPN for mobile robotic path planning research is performed by extending the concept of the Euclidean distance through considering the wireless packet losses with considering either ground or aerial robotics.

It is noted that the aerial wireless collection of ground-sensor data was found

with the use of fixed-wing UAVs by early researchers [e.g. [39]]. This approach, assuming that the fixed-wing UAV collects data instantly by merely flying through the neighborhood of the sensor nodes without hovering or turning, the classical Dubin's Travelling Salesman Problem with Neighborhood fits this situation. This problem has been researched by a number of researchers [40-42]. The downsides of these Dubin's TSPN/fixed-wing UAVs are two-fold. 1) They need a small airstrip to take off. 2) They cannot hover above the sensor nodes; therefore, if flying-through the sensors cannot successfully have sensor data transmitted, the fixed-wing needs to fly around and above the sensor with a large radius, which makes wireless communication more difficult and the energy consumption is much higher than expected. With the advent of more autonomous multi-rotor UAVs, these practical problems are resolved. In this paper, it is the multi-rotor UAVs that are concerned.

4.2.2 TSPN

The generic definition of TSPN was originally described by Arkin and Hassin [38]. The traditional TSPN optimization aims to provide the shortest Euclidean-distance based path to visit all the neighborhoods that envelop individual nodes.

The TSPN problem as the TSP problem is NP-hard and non-convex [38]. First of all, the solution to a TSPN problem has a long and rich history of studying. Numerous heuristic optimization and approximation methods ware proposed. In Arkin and Hassin (1994), a simple heuristic procedure for constructing tours was proposed, whose length is guaranteed to be within a constant factor of the length of an optimal tour [38]. Others, such as [119-123], attempted to improve the speed of finding the optimal solution.

Many heuristic methods have been proposed in the literature, which include the use of genetic programing, swarm intelligence methods (e.g. ant colony method), and evolutional methods [125, 126]. In general, this method lacks tractability and do not scale well when the number of nodes increase. Particularly, these methods do not fit the problem of focus in this paper, wherein the spatial path-energy expression includes two basic components.

Another school of optimization framework is to treat the problem as an non-convex mix-integer nonlinear programming (MINLP) problem. While MINLPs can be used for a variety of practical applications, problems with non-convex objective and constrains are much difficult to solve than the convex ones [127]. Only recently is the mix-integer non-linear programming method is introduced for solving the non-convex TSPN [128, 129]. In these efforts, they used a specific feature of the MINLP formulation when customizing the solver by adding specific 'cut' generators. Once all the binary variables in the formulation are fixed at 0 or 1, the continuous relaxation of the remaining problem is convex. It is thus possible to solve it to optimality using a continuous solver. In this work, the MINLP framework is adopted with a novel customization in expressing the total energy consumption of a UAV as a gateway in an AG-WSN network.

4.3 Formulation

4.3.1 Topological Configuration and Param

Since the shorter path is equivalent to less use of time and hence less energy

consumption, if without considering the hovering and the potential communication range, one may see that the solution to the shortest path is equivalent to that to the least energy consumption. In this paper, the focus is the energy optimization for a multi-rotor UAV that can stay hovering during the communication with a sensor node; therefore, the energy consumption to maintain the hovering is close to the consumption in the flying-forward mode [43]. As such, the energy consumed during this hovering time must be taken into consideration when optimizing the path. This also may imply that the shortest Euclidean-distance path does not necessarily mean the lowest energy consumption for the UAV.

Given an AG-WSN with an UAV as the gateway with n sensor nodes in the field, the UAV is assumed that it needs to visit all the n nodes once and only once in one trip to gather the sensing data through wireless communication. Figure 4.2 illustrates a conceptual geometry of the UAV and the sensor nodes. In Figure 4.2, the notion of the neighborhood of a sensor node i with its neighborhood, the impinging UAV, and the *effective* communication range is illustrated in terms of the radius distance d (e.g. $0 \leqslant d \leqslant d_{max}$), within which the critical variable d_0 is defined shortly.

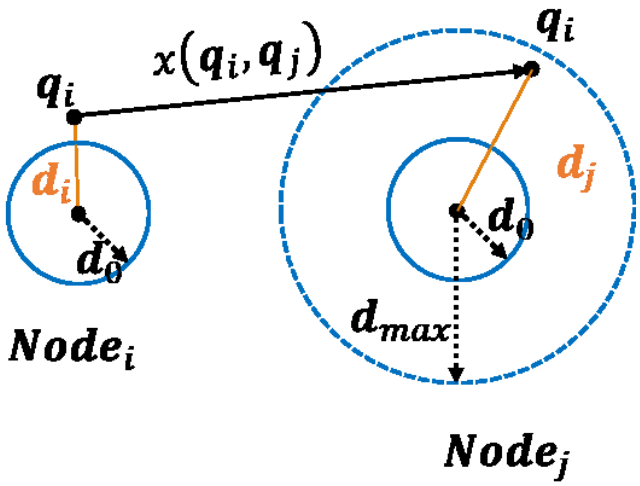

Figure 4.2. Illustration of two nodes of their neighborhood and UAV moving/hovering information.

The communication range between the UAV and sensor nodes is limited by many factors, which include power, obstacles, and antenna directions. This requires that the UAV approaches a sensor node i within the local neighborhood of Ω_i, which is a function of d_i, $\Omega_i = \Omega_i(d_i)$, around the sensor. In this paper, considering a perfect terrain without blocking and interfering, this local neighborhood (projected on the virtual configuration plane) is formed by a perfect circle and its enveloped area. The UAV then will hover at a selected point $q_i \in \Omega_i$ of the node i throughout data collection. It is mentioned that the limited UAV battery life requires the UAV reaching out to all the sensor nodes on the ground with the shortest path (hence the shortest flying time) to save the batter energy. Given the need of the traversal of all nodes and the definition of the neighborhoods of the nodes in Figure 4.2, this path planning for the UAV falls into the category of Travelling Salesman Problem with Neighborhood (TSPN).

Given Figure 4.2 (with two conceptual nodes, neighborhoods, and a path), the following variables are defined.

- $\boldsymbol{q}_i$,$\boldsymbol{q}_j$: UAV's hovering location (a coordinate vector) for the sensor node i,j;
- $\epsilon_{i,j}$: a binary variable that if there is any traveling path selected between the locations of $\boldsymbol{q}_i$ and $\boldsymbol{q}_j$ ($\epsilon_{i,j}$ =1, the path is selected; otherwise, not selected);
- $x(\boldsymbol{q}_i, \boldsymbol{q}_j)$: the spatial Euclidean distance from flying between the UAV hovering positions $\boldsymbol{q}_i$ and $\boldsymbol{q}_j$ corresponding to the node i and j, respectively, given a deterministic sensor network topology: $x(\boldsymbol{q}_i, \boldsymbol{q}_j) = \| \boldsymbol{q}_i - \boldsymbol{q}_j \|$, and it is noted that $x(\boldsymbol{q}_i, \boldsymbol{q}_j) = x(\boldsymbol{q}_j, \boldsymbol{q}_i)$.

To simplify the formulation, the major energy consumption activity of the UAV, which are the forward-moving and hovering modes driven by the motors, are considered. Other energy costs, including imaging, networking, and others are ignored.

4.3.2 Communication Range with Data Loss

Interference and packet loss is a common issue in WSN and has been well studied in the past [130-132]. Integrating a gateway device with a UAV makes the radio environment more complicated. The first reason is that the UAV communicates with its ground station using different wireless protocols than the WSN in the ground. It is common that the UAV with an imaging payload needs a high-power and high-throughput wireless protocol to send real-time video feeds back to the ground station, while the wireless communication for the WSN is low-power due to its low energy consumption requirements (hence low-power wireless protocols are often used, e.g.

ZigBee). The second reason is that two different wireless systems (with antennas) must be installed on the same multi-rotor UAV, which is often relatively in small size. The limited physical distance between the two wirelesses systems make the interference stronger on both ends.

This inference issue was explored in our recent work [48]. In this effort, the ZigBee-based WSN was adopted. The experimental evaluation indicated that when the UAV is equipped with both ZigBee and Wi-Fi modules, the ZigBee communication is heavily interference by the Wi-Fi signals. One of the most important conclusions is that, when measuring the Packet Delivery Ratio (PDR) between the UAV (with a Zigbee gateway) and the ground sensor node, the PDR in general decreases as the distance between the UAV and ground sensor node increases. The experimental relation is shown in Figure 4.3.

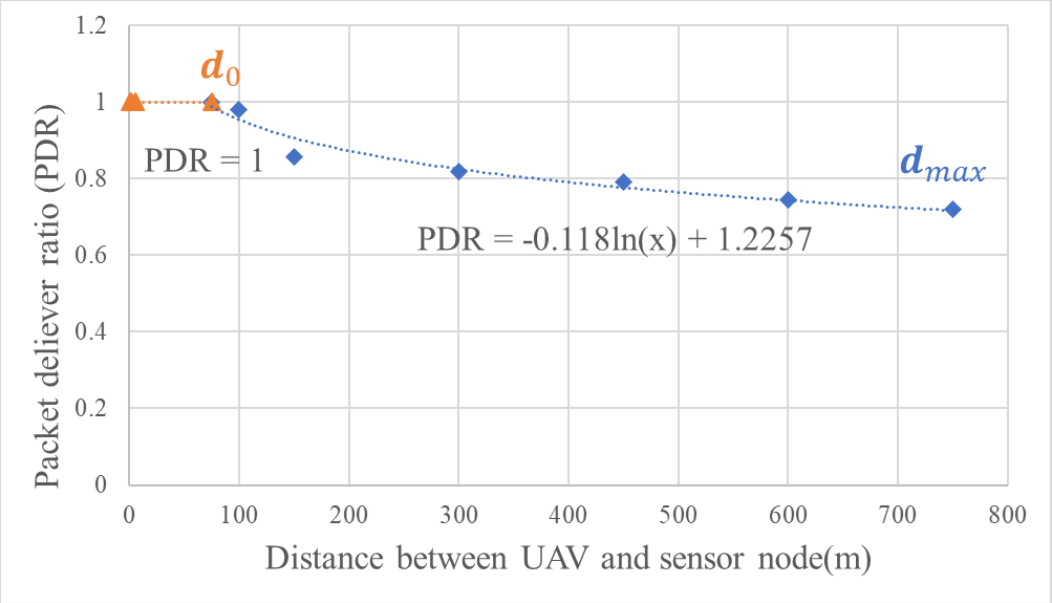

Figure 4.3. Experimental measured relations of package delivery ratio and the distance between the UAV and the ground sensor node.

The relation suggests that the UAV can achieve 100% PDR when the UAV is

largely within a certain radius of the ground sensor node. Beyond this radius, packet loss occurs during the communication. When this happens, the UAV needs to stay longer (hovering) till the lost packets are re-transmitted. Depends on several influential factors such as the distance and the relative orientation between the Wi-Fi and the Zigbee antennas, the UAV's video feed quality, the offset center frequency between Wi-Fi and Zigbee, or if a different wireless protocol is being deployed for WSN, the relation between the PDR and the distance could change accordingly. Nonetheless, it is asserted Figure 4.3 showcases a representative relation.

In this work, by observing Figure 4.3 two obvious segments of the relations exist, the empirical relation is simplified as follows:

1. If the distance d between the UAV and the sensor node is less than a certain deterministic range d_0 ($d \leqslant d_0$), which is the maximum radius for achieving the perfect data transmission (packet lossless radius), then it is assumed that there is no packet loss during the wireless communication. In this case, PDR always equal to 1.
2. If the distance d between UAV and the sensor node gets larger (i.e. $d > d_0$) the PDR will decrease as the distance increases. From our previous evaluation result, a logarithmic function has been found that fits the data well for the relation at this segment. In general, the equation is in the form of $PDR = \alpha \text{ Ln}(d) + \beta$, where α $\alpha$and β β are two function constants with $-1 < \alpha < 0$ $-1 < \alpha < 0$ and $d > d_0$.

In this work, the circle centering around a sensor node with the radius d_0 is

called the lossless zone (LLZ) (i.e. within an LLZ, the PDR retains as 1). Combining the above two parts, we can obtain the PDR as a function of the radius distance from the UAV to data transmission distance (d) as in Eq. 1, which will be used in the later discussion for the spatial path-energy optimization:

$$\boldsymbol{PDR} = \begin{cases} \mathbf{1}, & \boldsymbol{d \leq d_0} \\ \boldsymbol{\alpha\, ln(d) + \beta}, & \boldsymbol{d > d_0} \end{cases} \quad (1)$$

4.3.3 UAV Energy Consumption with Data Loss

The fundamental goal is to minimize the total energy of the UAV during a full traversal of the ground sensor nodes, denoted by E^T. To proceed with expressing the energy consumption in the UAV, the following simplification is introduced that the UAV flies with in a two-dimensional plane with a constant absolute height to the ground sensors (which are assumed in an absolute plane as well, Figure 4.1b). In addition, it is further assumed that a constant amount of data to be transferred for all sensor nodes. Given this, the total energy can be separated into two parts: the forward-moving E^f and the hovering-flying E^h. Assuming the rated power of the UAV in the forward-moving and the hovering modes, P_f and P_h, and the durations, T_f and T_h, respectively, the total energy cost is shown in Eq. 2.

$$\boldsymbol{E^T = E^h + E^f = P_h \times T_h + P_f + P_f} \quad (1)$$

Further, if the UAV stays hovering within an LLZ, $PRD(d) = 1$, the data transfer would take the constant time of T_0 (given the same amount of data to be transferred through all sensor nodes). If there is packet loss during the communication at the hovering mode (i.e. beyond the LLZ), the sensor node will re-transmit the lost packets

to the UAV. Ideally, the first attempt of the re-transmission will take the hovering time of $T_h = T_0 \times [1 - PRD(d)]$. Assuming the wireless protocol is designed in a way that multiple re-transmissions will be initiated till all the data is received by the gateway (in the UAV), the total transmission (hence the hovering time) can be calculated as Eq. 3, where, as $n \to \infty$ and considering $0 < PRD(d) < 1$, it reduces to:

$$\boldsymbol{T_h = T_0 \times [1 - PRD(d)] + T_0 \times [1 - PRD(d)]^2 + \cdots + T_0 \times [1 - PRD(d)]^n}$$

$$\boldsymbol{T_h = \frac{T_0}{PDR}} \tag{3}$$

Combining Eq. 1 and 3, therefore, the energy consumption for the UAV's hovering model when collecting data from one sensor becomes a piecewise function:

$$\boldsymbol{E^h = P_h \times \frac{T_0}{PDR(d)} = \begin{cases} P_h \times T_0 & d \le d_0 \\ P_h \times \dfrac{T_0}{\alpha\, ln(d) + \beta} & d > d_0 \end{cases}} \tag{4}$$

For the forward-moving paths, the time cost for a general path depends on the speed and the path distance. Assuming the forward-moving speed is v_f and a path distance x, the general forward-moving energy cost is:

$$\boldsymbol{E^f = P_f \times \frac{x}{v_f}} \tag{5}$$

which is defined physically as the product of the select path distance normalized by the forward-moving speed v_f, giving out the flight time, and the UAV's forward-moving power P_f. From Eq. (4) and (5), it is obvious that without considering the forward-moving travel to the sensor nodes, if only the E^h is taken into account, the total minimal of E^h can be achieved by setting $d \leqslant d_0$ to achieve the shorter hovering time

for all individual sensor nodes. This, however, requires the UAV travels a longer distance to be within the LLZs of all sensors, which leads to longer paths and greater energy consumption in the E^f part of the complete trip. This situation demands a trade-off in general in deciding the amount of hovering and the mount of forward-moving; and granularly, this may vary significantly depending the topology of the ground network and the param in Eq. 4 and 5.

4.3.4 MINLP Formulation and Solution Classification

Given the set of $\boldsymbol{\mathcal{N}} = \{1,2,\dots,n\}$ representing all the sensor nodes to be visited, based on the standard non-convex MINLP formulation as shown in [128], the proposed spatial path-energy optimization is proposed, firstly in general, both the forward-moving and the hovering-triggered energy costs are summed. To encode the paths that are travelled by the UAV, the binary variables set $\{\epsilon_{i,j} \mid i = 1, 2, \dots, n; j = 1, 2, \dots, n, \text{ and } i \neq j\}$ is used to mark the paths selected ($\epsilon_{i,j} = 1$); the location vector variables $\{\boldsymbol{q}_i \mid i = 1, 2, \dots n\}$ are used to mark the location selected ($\boldsymbol{q}_i$) within the neighborhood of Ω_i that is further defined by the radius distance d_i. With these notions and based on the general concept in Eq. 2, Table 4.1 defines all the solution frameworks proposed in this paper. The definitions in details and explanations are given following Table 4.1.

Table 4.1. Proposed 2-D spatial path-energy optimization through a non-convex Mixed Integer Nonlinear Programing framework.

Minimize [1]	$\sum_{i=1}^{n}\sum_{\substack{j=1 \\ j\neq i}}^{n} \varepsilon_{ij} \times P_f \times \frac{x(\boldsymbol{q}_i, \boldsymbol{q}_j)}{v_f} + \sum_{i=1}^{n} P_h \times \frac{T_0}{PDR(d_i)}$	(6)
Minimize [1]	$\sum_{i=1}^{n}\sum_{\substack{j=1 \\ j\neq i}}^{n} \varepsilon_{ij} \times x(\boldsymbol{q}_i, \boldsymbol{q}_j) + v\, T_0 \sum_{i=1}^{n} \frac{1}{PDR(d_i)}$	(7)
Minimize [1]	$\sum_{i=1}^{n}\sum_{\substack{j=1 \\ j\neq i}}^{n} \varepsilon_{ij} \times x(\boldsymbol{q}_i, \boldsymbol{q}_j)$	(8)

Subject to

C1	$\sum_{j=1}^{i-1} \varepsilon_{ji} + \sum_{j=i+1}^{n} \varepsilon_{ij} = 2 \quad \forall i \in \boldsymbol{\mathcal{N}}$	(9)
C2	$\sum_{i\in S} \left(\sum_{\substack{j\in N\setminus S \\ j<i}} \varepsilon_{ji} + \sum_{\substack{j\in N\setminus S \\ j>i}} \varepsilon_{ij} \right) \geq 2 \quad \forall S \subset \boldsymbol{\mathcal{N}}\setminus\{1\}, \lvert S\rvert \geq 3$	(10)
C3	$\varepsilon_{ii} = 0 \quad \forall i \in \boldsymbol{\mathcal{N}}$	(11)
C4	$\varepsilon_{ij} + \varepsilon_{ji} \leq 1 \quad \forall i, j \in \boldsymbol{\mathcal{N}}$	(12)
[2]C5	$q_i \in \Omega_i \quad \forall i \in \boldsymbol{\mathcal{N}}$	(13)
C6	$\varepsilon_{ij} \in \{0,1\} \quad \forall i, j \in \boldsymbol{\mathcal{N}}, j > i$	(14)

To solve $\{\epsilon_{i,j} \mid i = 1, 2, \ldots, n; j = 1, 2, \ldots, n, \text{ and } i \neq j\}$ and $\{(\boldsymbol{q}_i, d_i) \mid i = 1, 2, \ldots, n\}$.

Note:

1. The objective functions in Eq. 6 and 7 are equivalent when assuming $v_f = v_h$ and $P_f = P_h$, which defines the dynamic optimized path-energy solution; and the objective function in Eq. 8 defines the shortest-path solutions.
2. The neighborhood in C5, Ω_i, is unified as either $\Omega(d_0)$ or $\Omega(d_{max})$, depending on the solution framework.

First, a novel and generalized objective function is proposed in Eq. 6. This objective function comprises two summation terms with the first being the total summed forward-moving energy cost by traveling to all the local neighborhoods following a selected path scenario, and the second term being the total summed hovering induced energy cost for which the hovering time depends on the communication packet delivery rate function $PDR(d_i)$. Eqs. 9 to 14 further define the constraints (C1 to C6) that provide restriction in searching for the optimum of $\epsilon_{i,j}$'s, $\boldsymbol{q}_i$'s, and the associated d_i's. Table 4.1 summarizes the completed expressions for executing the nonconvex MINLP optimization framework.

Among the constraints C1 to C6, the constraint C1 ensures that each node is visited once and only once by the UAV. C2 eliminate any sub-tour by forcing the number of active edges departing from any subgraph induced by a subset of the vertices with cardinality at least 2 to be at least equal to 1 [128]. Constrains C3 and C4 prevent the node from connecting to itself, as well as from two nodes forming a circle. C5 defines the neighborhood for each sensor node (a critical condition to be elaborated later); and C6 makes sure ε_{ij} is binary.

Several parametric assumptions can be made for achieving the simplicity yet without losing the generality:

1. The unit power of the UAV remains a constant during the hovering and forward-moving modes; hence, $P_f = P_h = P$;
2. The speed of the UAV remains a constant during forward-moving modes; hence, $v_f = v$;

In reality, one may assume that the hovering power (or speed) is only a fraction of the forward-moving power (or speed), namely $v_h = \gamma_1 v_f$ or $P_f = \gamma_2 P_h$, respectively; and similar simplification can be achieved as well. These two parametric assumptions will simplify the expression of the resulting objective function (Eq. 7) with the same constraints previously.

Given the objective function in Eq. 6 or 7, it is noted that this differs from the standard objective function in the literature [128]. In a standard TSPN problem, the objective function is simply defined as the cumulative summation of all selected paths between the selected locations (i.e. the first term in Eq. 7). The Euclidian distance $x(\boldsymbol{q}_i, \boldsymbol{q}_j)$ hides a pivotal variable – the radius distance between the sensor nodes and the UAV, correspondingly d_i and d_j, respectively; as shown in Figure 4.2, the variable d_i and d_j values modify nonlinearly the Euclidian distance $x(\boldsymbol{q}_i, \boldsymbol{q}_j)$. Herein, to achieve the optimal (minimized) path-energy cost, the energy cost due to the hovering and data collection is added in addition to the forward-moving traversal of all sensor neighborhoods. As qualitatively implied earlier and further evidenced in Eq. 6 or 7, there exists a dynamic balance between minimizing the shortest paths only hence less in forward-moving traveling energy cost (the first term in Eq. 6 or 7;) and minimizing the hovering energy cost (the second term in Eq. 6 or 7).

In addition, it is recognized that in a standard TSPN problem, the neighborhood for each target location (Ω_i) is user-defined with a fixed local area has been outlined (considering other conditions). For the UAV serving as a gateway to receive data from the ground sensors, there are no such pre-defined neighborhoods. Based on the *PDR*

function in Figure 4.3, two critical neighborhoods are recognized: the neighborhoods defined by the aforementioned LLZ radius d_0, defined by $\Omega(d_0)$; and further, by assuming a maximal packet loss radius (based on an empirical justification) d_{max}, at which the packet delivery rate is as the smallest as to maintain an effective communication link, a maximal packet-loss neighborhood $\Omega(d_{max})$ is defined. In the meantime, one can practically define that these neighborhoods do not overlap between nodes.

With the insight into the possible tradeoff between the forward-moving traveling energy cost and the hovering energy cost, and the flexibility in defining the local neighborhoods, two possible lower-bound solutions are derived. First, one seeks to minimize the forward-moving traveling energy cost (Eq. 8), namely the shortest-path solution; then by setting the local neighborhoods, two bound solutions are obtained:

1. Set $\Omega_i = \Omega(d_0)$, namely all local neighborhoods assume the same circular local region defined by the LLZ radius d_0. By taking this neighborhood setting, for all sensor nodes, the data communication is lossless hence the hovering time is less; hence the resulting solution is called Lossless Shortest-path (LL-SP) solution in this paper. This solution tends to give rise to less hovering energy cost.
2. Set $\Omega_i = \Omega(d_{max})$, namely all local neighborhoods assume the same circular local region defined by the maximal-loss radius d_{max}. By taking this neighborhood setting, for all sensor nodes, the data communication within this neighborhood possibly encounters maximal loss. However,

the total traversal paths across all sensor nodes may be smaller than the solution above (due to the larger neighborhood size); therefore, the total energy cost may still poise to be a lower-bound. This resulting solution is called Maximal-loss Shortest-path (ML-SP) solution in this paper. This solution tends to give rise to less forward-moving energy cost.

To carry out the originally proposed spatial path-energy optimization expressed in the objective function in Eq. 7 and to have a fair comparison with the above two shortest-path solutions, the local subdomains Ω_i is set equal to $\Omega(d_{max})$ as well. However, as expressed earlier, this solution emphasizes a dynamic balance through minimizing the total energy cost including both the forward-moving and hovering of the UAV. This solution is called *dynamically minimized path-energy* (DM-PE) solution.

If all the three solution frameworks are solved through the MINLP procedure, denoted by $\{\boldsymbol{q}_i^*, d_i^*, \epsilon_{i,j}^* | \ i = 1, 2, \ldots, n; j = 1, 2, \ldots, n, j \neq i\}$, the total energy (subject to multiplying the force constant P/v) can be inserted in the objective functions. Noted that when using Eq. 8, the constant energy term due to the hovering needs to be added back. This uniform total 'energy' function (subject to a constant multiplier P/v) is shown below in Eq. 15. It is noted that in this equation, the optimized radius distances (d_i^*,) for all sensor nodes are explicitly expressed in the optimized UAV locations $\boldsymbol{q}_i^*$'s.

$$\boldsymbol{E^T} = \sum_{i=1}^{n} \sum_{\substack{j=1 \\ j \neq i}}^{n} \boldsymbol{\varepsilon_{ij}} \times \boldsymbol{x}\left(\boldsymbol{q_i^*}\,[\boldsymbol{d_i^*}], \boldsymbol{q_j^*}[\boldsymbol{d_j^*}]\right) + \boldsymbol{v}\ \boldsymbol{T_0} \sum_{i=1}^{n} \frac{\mathbf{1}}{\boldsymbol{PDR}(\boldsymbol{d_i}^*)} \tag{15}$$

With the three solution frameworks, the resulting total energy quantities are termed E_{LL-SP}^T , E_{ML-SP}^T, and E_{DM-PE}^T, respectively.

With the three total energy costs, and given the objective is to find the minimum of the total energy cost, it is desirable to rank them without numerical evaluation. However, due to the complexity in the nonlinearity in defining the objective function and further due to the unforeseen possibility of the spatial topology of the ground sensor network, it is unfortunate that no deterministic ranking is possible. The least insight as previously pointed out is that either the LL-SP or the ML-SP solution may offer a lower-bound energy cost.

From an optimization, theoretic point of view, the second term in Eq. 7 acts like a regularization term. In addition, the second term is necessary in calculating the total energy, even the shortest-path solutions are used. From this insight, the product term v T_0, denoted by $\lambda = v\ T0$, which physically equivalent to the flight distance if the UAV flies instead of hovering given a speed of v and a time of T_0 (the data transmission time). The summation term ($\sum_{i=1}^{n} \frac{1}{PDR(d_i^*)}$) hence acts as the 'penalty' function, which imposes additional 'path' cost to the total forward-moving traversal energy cost. This λ, termed the path-energy control parameter, therefore is worthy of parametric investigation in accordance with its physical meaning. Comprehensive numerical evaluation and the advantage of the proposed DM-PE solution are offered below.

4.4 Implementation and Numerical Evaluation

4.4.1 Optimization Package and Implementation

We use Julia Programming Language as our programming environment, and Juniper [133], a nonlinear branch-and-bound solver for our calculation. Juniper (Jump Non-linear Integer Program solver) is a solver for Mixed Integer Non-Linear Programs

(MINLPs) written in Julia. Juniper solves these kinds of problems using an NLP solver and then branch and bound. If the NLP solver isn't global optimal then Juniper is a heuristic.

4.4.2 Simple Examples

Following the previously defined optimization schemes in Table 4.1, the goal here is to compare the differences of the solution using three different optimization schemes and compare the total energy costs. First, the following network param are selected listed in Table 4.2 (for α, β, d_0 and d_{max}).

Table 4.2 Numerical value of the network param.

Parameter	Value
α	-0.118
β	1.225
d_0	50
d_{max}	500

A simple 10-node instance is devised in this experiment. The LLZ radius d_0 equals to 50 m, and the practical maximum data transmission range d_{max} is 500 m. Using this setup, the three optimization schemes (LL-SP, ML-SP, and DM-PE) are obtained. The results with the achieved traveling graphs are shown in Figure 4.4 and Table 4.3.

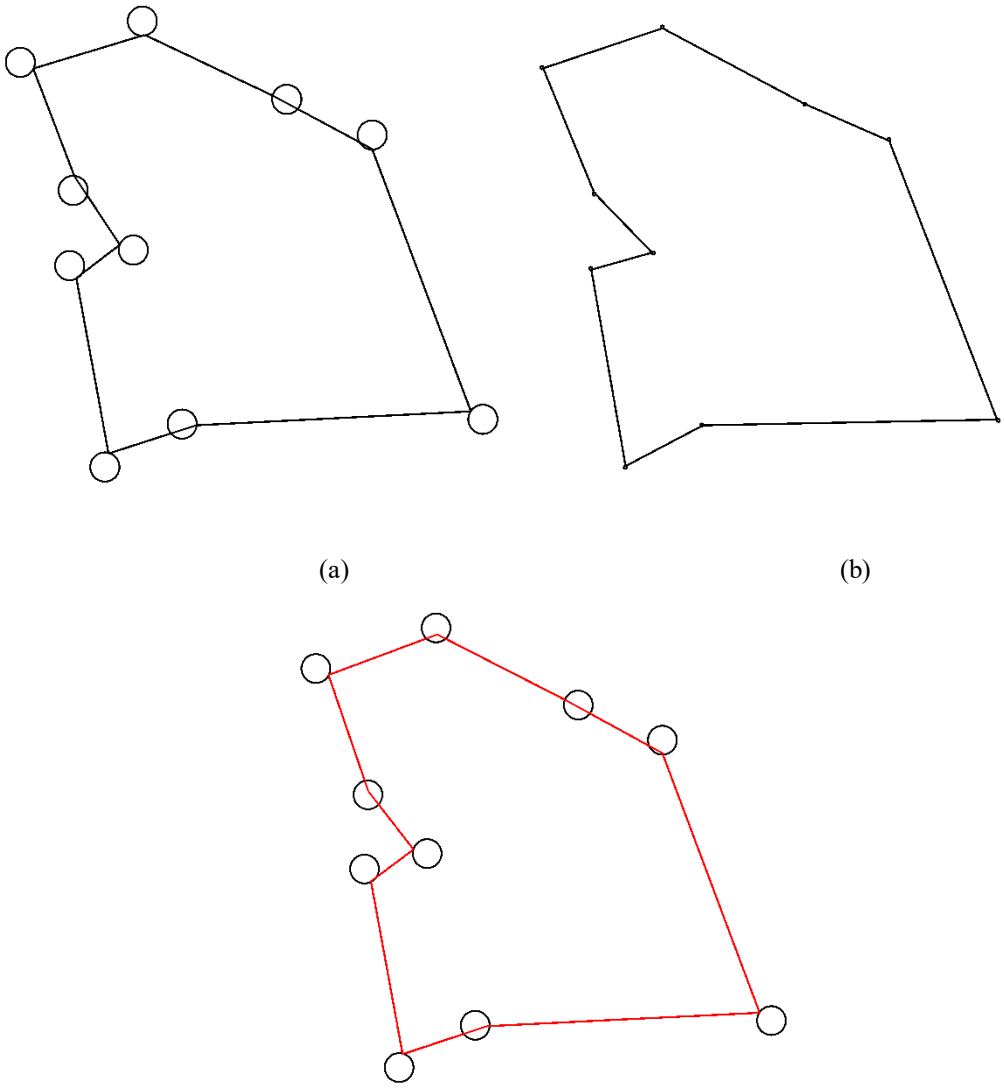

(a) (b)

(c)

Figure 4.4 A 10-Node sensor network simulation: (a) LL-SP; (b) ML-SP; and (c) DM-PE. Note that the larger circles shown in the graphs have a radius of 500 m (d_{max} = 500 m); and the smaller is d_0 = 50 m.

Table 4.3 The total 'energy' cost in details from the three different solutions.

Optimization Scheme	E^T_{ML-SP}		E^T_{DM-PE}		E^T_{LL-SP}	
Mode	Forward Moving	Hovering	Forward Moving	Hovering	Forward Moving	Hovering
Energy Cost	50877	13100	51143	12695	54745	10000
Total Energy	63977		63838		64745	

The different resulting traveling paths clearly show that the results are much different. The proposed DM-PE optimization scheme, which show in Figure 4.4(c), suggests that the UAV should neither use the d_{max} nor d_0 as neighborhood radius and using a traditional TSPN solution. The UAV should hover between d_0 and d_{max}. The location is determined by the parameter values of α, β, d_0, v and T_0. From equation 1 we know that α, β and d_0 are related to wireless communication hardware and cannot be changed once the hardware is implemented. The product of v and T_0 is another important factor to determine where the UAV should hover: The larger the product, the more energy is consumed during the hovering states, thus we want the UAV fly closer to the node, in extreme case, our approach will have the same result as the Lossless approach. On the contrary, if the product of v and T_0 is small, we want less UAV travel distance and hover further from the node. In extreme case, our approach will have the same result as the Shortest distance approach.

4.4.3 Large-scale Examples

To maximize the similarity between our simulation and the real applications, we generate 173 nodes located in a 20000 square meter area. Each node is at least 100 m away from the nearest neighbor to make sure their neighborhood does not overlap. From the 173 nodes set, we randomly pick 10, 15, 20 … nodes as our node map to run the simulation. The following tables (Table 4.4 to Table 4.6) show the total energy of different nodes and approaches. In each table, the left column is the total number of the nodes for each simulation instance; each row shows the total "energy" for different approaches, the numerical value "energy" represents the sum of Euclidean distance and

virtual distance convert from equation 14. The lower the value, the lower total energy consumption is for that method.

Table 4.4 Total energy of different nodes and approaches, $\lambda = 1500$

Node	E^T_{ML-SP}	E^T_{DM-PE}	E^T_{LL-SP}
10	70526	69745	69745
15	92115	92081	92081
20	106984	104937	104937
25	130297	128084	128084
30	148711	146441	146441
35	151166	146727	146727
40	167400	162856	162856

Table 4.5 Total energy of different nodes and approaches, $\lambda = 1200$

Node	E^T_{ML-SP}	E^T_{DM-PE}	E^T_{LL-SP}
10	66596	66377	66745
15	86220	86220	87581
20	99149	98478	98937
25	120472	119920	120584
30	137036	137036	137441
35	137422	136227	136227
40	151784	148785	150856

Table 4.6 Total energy of different nodes and approaches, $\lambda = 1000$

Node	E^T_{ML-SP}	E^T_{DM-PE}	E^T_{LL-SP}
10	63977	63838	64745
15	82290	84255	84581
20	93926	93562	94937
25	113922	113772	115584
30	129253	129253	131441
35	128259	128259	129227
40	141374	139381	142856

Table 4.7 Total energy of different nodes and approaches, $\lambda = 800$

Node	E^T_{ML-SP}	E^T_{DM-PE}	E^T_{LL-SP}
10	61356	61299	62745
15	78360	78360	81581
20	88703	88645	90937
25	107372	107372	110584
30	121470	121470	125441
35	119096	119096	122227
40	130964	129976	134856

Table 4.6 Total energy of different nodes and approaches, $\lambda = 500$

Node	E^T_{ML-SP}	E^T_{DM-PE}	E^T_{LL-SP}
10	57426	57426	59745
15	72465	72465	77081
20	80868	80868	84937
25	97548	97548	103084
30	109796	109796	116441
35	105352	105352	111727
40	115349	115349	122856

In these tables, the lowest value of each row is highlighted. We can see that depends on the product of $\boldsymbol{v} \times \boldsymbol{T_0}$, our approach may fall back into the Lossless or the Shortest distance solution. It proves our assumption that when $\boldsymbol{v} \times \boldsymbol{T_0}$ is small, our approach (dynamic) will be similar or the same as the Shortest distance approach, while $\boldsymbol{v} \times \boldsymbol{T_0}$ is large, our approach will be similar or the same as the Lossless approach, and if $\boldsymbol{v} \times \boldsymbol{T_0}$ is in a middle range of the two extreme, the dynamic approach will have a better result than the other two. A visualized example is chosen from Table 4.4, $\boldsymbol{v} \times \boldsymbol{T_0} = 800$ Node = 40, Figure 4.5

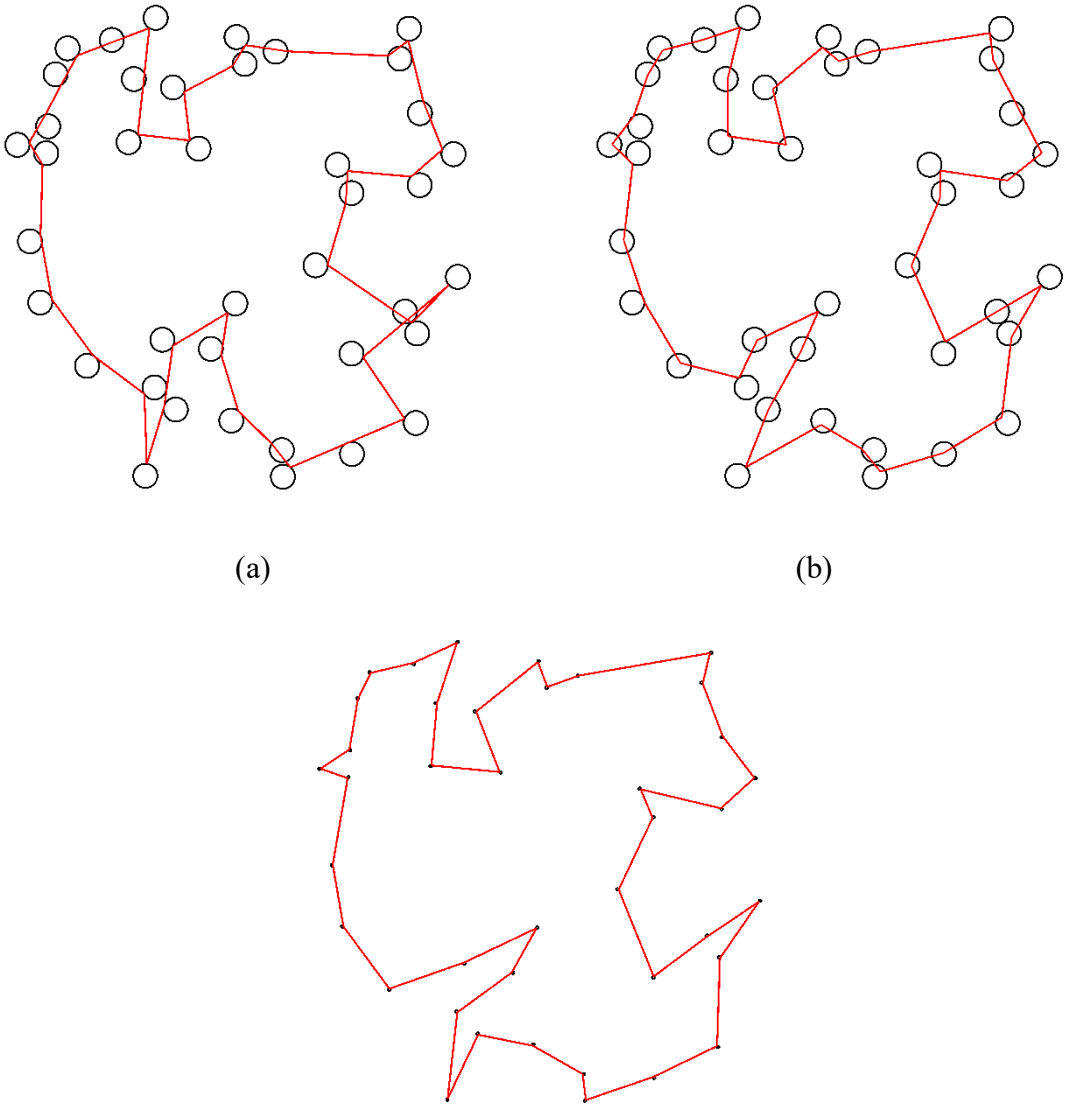

(a) (b)

(c)

Figure 4.5 A 20km by 20km map with 40 nodes. Each node is at least 1000 meters away from each other. (a) Shortest distance approach, UAV try to "touch" the 500-meter radius circle of each node, and then head to the next target node. (b) Our dynamic approach, the 500-meter radius circle for each node is an upper boundary, the UAV can go into the circle to achieve better wireless communication condition. (c) Lossless approach, UAV will get very close to the node (within 50 meters radius), to ensure no packet loss occur during wireless communication between UAV and node. Note that on the image these circles in (c) is tiny since 50 meters is relatively small on a $20km^2$ map.

4.4.4 Observed Computational Cost

The simulation in Section 5 runs on PC with Windows 10, CPU i7-6700k (4.4GHz clock, 4 cores, 8M Cache), and 16G memory. Table 4.7 shows the computing

time for the three methods with different nodes topology.

Table 4.7 Computational cost in second

Node number	ML-SP	DM-PE	LL-SP
10	0.5	0.49	0.56
15	23.72	23.16	49.07
20	3.2	2.82	3.07
25	7.07	12.61	5.07
30	38.08	39.33	7.59
35	127.02	207.3	46.62
40	2749.5	356.67	227.4

The code is not optimized for parallel computing thus only 1 core is used during the simulation. We also find when we increase the number of nodes from 40 to 45, the calculation time roughly increased from a few minutes to a few hours with our current hardware set up. This maybe solved be using different workstation and adding parallel computing capability with the Julia code, however, optimize the NP-hard computing time is not the focus of this work.

4.6 Conclusions and Remarks

Our initial goal is to minimize the energy consumption for the UAV by optimize the flying path. We recognize traditional TSPN solution is not suitable for real application since packet loss in wireless communication is not considered. Therefore, we proposed the new dynamic TSPN approach to address the problem. The dynamic approach modifies existing mixed-integer non-linear programming TSPN solution, adding parameters that reflects wireless packet loss the hovering state energy consumption. Simulation results indicates the dynamic approach will provide lower

total energy consumption solution than the other two approaches in certain conditions.

Notice our approach sometimes will have the same result as either the Lossless approach, or the Shortest distance approach. The key parameter for a known nodes map is the products of $\boldsymbol{v} \times \boldsymbol{T_0}$, in other words, the wireless data packet size and the UAV flying velocity. We conclude that for real applications, once all the parameters is settled, we can use the dynamic approach to find the lowest energy path for the UAV, and then start the flight mission.

Another limitation for this work is the parameters $\boldsymbol{\alpha}, \boldsymbol{\beta}$, and equation 1 are experimental results from our previous work, this will change on different hardware set up. To apply our dynamic approach, one needs to know these parameters for the specific set up.

CHAPTER 5

CONCLUSION AND FUTURE WORK

5.1 Conclusion

In this dissertation, a novel aerial-ground wireless sensing network (AG-WSN) that aims to transform a number of critical geospatial sensing and monitoring practices, such as precision agriculture, civil infrastructure protection, and disaster response, is developed. To achieve maximal energy efficiency, three research problems are concerned in this dissertation.

First, a radio-frequency (RF) wake-up mechanism is investigated for aerial activation of ground sensors using a UAV platform. In this section, we reviewed and compared different wake-up mechanism for WSN and chose active radio frequency based wake-up method and implemented physically. We find that the RF-based out-band wake-up mechanism can save a great deal of energy compared with the other two solutions (the infrared wake-up and the default duty-cycle methods).The results show that the RF-based wake-up mechanism can potentially save more than 98.4% of the energy that the traditional duty-cycle method would otherwise consume, and 96.8% if an infrared-receiver method is used.

Based on this setup, the delay of wake-up is also studied by using high speed camera. The results indicate with a variety of wake-up RF signal combination, the delay is less than 80 milliseconds hence will not affect the overall opportunistic sensing applications.

Second, the data transmission under wireless interference between the UAV and

ground WSN, specifically between Wi-Fi and ZigBee, is experimentally investigated. It is observed that the relative position of the Wi-Fi and ZigBee antennas and the distance between them are the two major factors that impact the communication. In the long-range experiment, the ZigBee data transmission is tested as the range varies up to 800 meters (the line-of-sight distance). Defining the range with the packet delivery rate of 99.8% as the ZigBee 'comfort zone', the effect of the ZigBee/Wi-Fi antenna distance is further determined and recognized as a sensitive parameter. It is found that with a few centimeters of increment in this distance, the comfort zone range can be improved significantly. These results provide the guideline in designing the mixed communication configuration in deploying the proposed aerial-ground sensing network wherein Wi-Fi and ZigBee networking are both involved, especially when the ranges of operating frequencies at both overlap. Besides that, finding of the relation between Zigbee packet loss and distance provides an important parameter for the last part of the dissertation research.

Last, this dissertation theoretically explores and develops an optimization framework for UAV's aerial path planning when collecting ground-sensor data. We recognize traditional TSPN solution is not suitable for real application since packet loss in wireless communication is not considered. Therefore, we proposed the new Dynamic TSPN approach to address the problem, which used an improved mixed-integer non-linear programming approach. Simulation results indicates the Dynamic approach will provide lower total energy consumption solution than the other two approaches in certain conditions.

We find that the products of $\boldsymbol{v} \times \boldsymbol{T_0}$, in other words, the wireless data packet size and the UAV flying velocity is a key parameter that may have impact the optimization solution. Thus, we suggest for real application this value should be determined carefully before each flight mission.

5.2 Future Work

There are several future tasks are identified through the dissertation.

1. The method to evaluate the energy consumption of wireless sensor node in this work is at a higher level, which provides the number of days the sensor node can work until it turns off. An alternative approach would be using high accuracy bench digital meters, to provide real-time power consumption of the node, which can further strength our assumptions that RF wake-up mechanism is at advantage of other methods.
2. The experimental in Chapter 3 is based on the commercially available DJI drone and hence is not a platform suitable for developments. The Wi-Fi parameter on that platform is not in our control, thus we did not conduct experiments on how the Wi-Fi video feed quality and the power level for both Wi-Fi and Zigbee radio will affect the interference level. Further work can be done using a customizable UAV platform with different Wi-Fi modules.
3. It is noted that Chapter 3 focuses on defining the concept of the aerial-ground wireless sensing and investigating the network interference within such a novel network, realistic structural response and environmental data are not analyzed. The future efforts based on finding in this include the development of heterogeneous

sensing including low-speed environmental sensing (e.g. temperature and moisture data at a rate of one data point per minute) and fast structural sensing (e.g. acceleration data at a rate of 200 points per second), and the aerial real-time data acquisition and computing. The subsequent investigation will include the implementation of a decentralized sensing solution that is optimized for either a single large-scale structure or a geospatially-large structure clusters in an urban area. The implementation task further includes the edge-computing based data processing and system identification towards fully real-time flying, sensing, and delivering of structural health and condition assessment analytics.

4. Simulation in Chapter 5 is using Julia programming language, the code is not optimized for parallel computing, which results running on a multi-core multi-threads CPU cannot improve the computation time. One possible improvement would be optimizing the coding for parallel computing.
5. The result on energy consumption indicate that across the different approach, the total energy difference is not huge compare to their total value. This may lead to a debate that whether it is worth of trying to compute for the optimization path since it may cost more energy for compute than it saves. We believe this can be further investigated by take the computing cost into consider and compare the energy cost to the UAV flying energy.
6. Some parameter provides to run the simulation in Chapter 5 are based on the experiments done in Chapter 4. Thus, it only provides one possible wireless packet loss model. We suggest other researches could conduct more experiments with

different hardware setup to get different model of wireless packet loss relative to distance. Then apply our dynamic approach to evaluate the energy consumption results with our setup.

REFERENCES

[1] L. Ruiz-Garcia, L. Lunadei, P. Barreiro, and I. Robla, "A review of wireless sensor technologies and applications in agriculture and food industry: state of the art and current trends," *Sensors,* vol. 9, no. 6, pp. 4728-4750, 2009.

[2] The Economist. (2017). *Superstructures*. Available: https://www.economist.com/node/17647603

[3] C. Pohl and J. L. Van Genderen, "Review article multisensor image fusion in remote sensing: concepts, methods and applications," *International Journal of Remote Sensing,* vol. 19, no. 5, pp. 823-854, 1998.

[4] A. Singh, "Review article digital change detection techniques using remotely-sensed data," *International Journal of Remote Sensing,* vol. 10, no. 6, pp. 989-1003, 1989.

[5] F. Y. Narvaez, G. Reina, M. Torres-Torriti, G. Kantor, and F. A. Cheein, "A Survey of Ranging and Imaging Techniques for Precision Agriculture Phenotyping," *IEEE/ASME Transactions on Mechatronics,* vol. 22, no. 6, pp. 2428-2439, 2017.

[6] I. Colomina and P. Molina, "Unmanned aerial systems for photogrammetry and remote sensing: A review," *ISPRS Journal of Photogrammetry and Remote Sensing,* vol. 92, pp. 79-97, 2014.

[7] C. Zhang and J. M. Kovacs, "The application of small unmanned aerial systems for precision agriculture: a review," *Precision Agriculture,* vol. 13, no. 6, pp. 693-712, 2012.

[8] E. Kayacan, H. Ramon, and W. Saeys, "Robust trajectory tracking error model-based predictive control for unmanned ground vehicles," *IEEE/ASME Transactions on Mechatronics,* vol. 21, no. 2, pp. 806-814, 2016.

[9] A. Baggio, "Wireless sensor networks in precision agriculture," in *ACM Workshop on Real-World Wireless Sensor Networks (REALWSN 2005), Stockholm, Sweden*, 2005, pp. 1567-1576.

[10] X. Dong, M. C. Vuran, and S. Irmak, "Autonomous precision agriculture through integration of wireless underground sensor networks with center pivot irrigation systems," *Ad Hoc Networks,* vol. 11, no. 7, pp. 1975-1987, 9// 2013.

[11] N. Wang, N. Zhang, and M. Wang, "Wireless sensors in agriculture and food industry—Recent development and future perspective," *Computers and Electronics in Agriculture,* vol. 50, no. 1, pp. 1-14, 1// 2006.

[12] N. Dlodlo and J. Kalezhi, "The internet of things in agriculture for sustainable rural development," in *Emerging Trends in Networks and Computer Communications (ETNCC), 2015 International Conference on*, 2015, pp. 13-18: IEEE.

[13] J. Ma, X. Zhou, S. Li, and Z. Li, "Connecting agriculture to the internet of things through sensor networks," in *Internet of Things (iThings/CPSCom), 2011 International Conference on and 4th International Conference on Cyber, Physical and Social Computing*, 2011, pp. 184-187: IEEE.

[14] J. P. Lynch and K. J. Loh, "A summary review of wireless sensors and sensor

networks for structural health monitoring," *Shock and Vibration Digest,* vol. 38, no. 2, pp. 91-130, 2006.

[15] Y. Gao, B. Spencer, and M. Ruiz-Sandoval, "Distributed computing strategy for structural health monitoring," *Structural Control and Health Monitoring,* vol. 13, no. 1, pp. 488-507, 2006.

[16] T. Nagayama and B. F. Spencer Jr, "Structural health monitoring using smart sensors," Newmark Structural Engineering Laboratory. University of Illinois at Urbana-Champaign.1940-9826, 2007.

[17] Y. Wang, J. P. Lynch, and K. H. Law, "A wireless structural health monitoring system with multithreaded sensing devices: design and validation," *Structure and Infrastructure Engineering,* vol. 3, no. 2, pp. 103-120, 2007.

[18] G. Morgenthal and N. Hallermann, "Quality assessment of unmanned aerial vehicle (UAV) based visual inspection of structures," *Advances in Structural Engineering,* vol. 17, no. 3, pp. 289-302, 2014.

[19] N. Metni and T. Hamel, "A UAV for bridge inspection: Visual servoing control law with orientation limits," *Automation in Construction,* vol. 17, no. 1, pp. 3-10, 2007.

[20] C. M. Yeum and S. J. Dyke, "Vision-based automated crack detection for bridge inspection," *Computer-Aided Civil and Infrastructure Engineering,* vol. 30, no. 10, pp. 759-770, 2015.

[21] H. Yoon and B. F. Spencer Jr, "Enabling smart city resilience: Post-disaster response and structural health monitoring," Newmark Structural Engineering Laboratory. University of Illinois at Urbana-Champaign.1940-9826, 2016.

[22] M. Collotta, L. Gentile, G. Pau, and G. Scatà, "A dynamic algorithm to improve industrial wireless sensor networks management," in *IECON 2012-38th Annual Conference on IEEE Industrial Electronics Society*, 2012, pp. 2802-2807: IEEE.

[23] D. Setiawan, A. A. Aziz, D. I. Kim, and K. W. Choi, "Experiment, modeling, and analysis of wireless-powered sensor network for energy neutral power management," *IEEE Systems Journal,* 2017.

[24] J. Zhao, L. Yao, R.-F. Xue, P. Li, M. Je, and Y. P. Xu, "An integrated wireless power management and data telemetry IC for high-compliance-voltage electrical stimulation applications," *IEEE Transactions on Biomedical Circuits and Systems,* vol. 10, no. 1, pp. 113-124, 2016.

[25] D. He and B. Fahimi, "Power management of a self-powered multi-parameter wireless sensor for IoT application," in *Applied Power Electronics Conference and Exposition (APEC), 2018 IEEE*, 2018, pp. 1380-1385: IEEE.

[26] J. Chen and Z. Chen, "Sensor Wake-up Implementation in Wireless Aerial-ground Sensing and Comparative Evaluation," *IEEE/ASME Transactions on Mechatronics* p. In Review, 2018.

[27] K. Fodor and A. Vidács, "Efficient routing to mobile sinks in wireless sensor networks," in *Proceedings of the 3rd International Conference on Wireless Internet*, 2007, p. 32: ICST (Institute for Computer Sciences, Social-Informatics and Telecommunications Engineering).

[28] E. Pignaton de Freitas *et al.*, "UAV relay network to support WSN connectivity,"

in *Ultra Modern Telecommunications and Control Systems and Workshops (ICUMT), 2010 International Congress on*, 2010, pp. 309-314: IEEE.

[29] Z. Chen, J. Chen, and C. Chase, "Robotic Aerial-Imaging and Ground-Sensing Network for Use in Rapid Emergency Response," presented at the The Joint 6th International Conference on Advances in Experimental Structural Engineering (6AESE) and 11th International Workshop on Advanced Smart Materials and Smart Structures Technology (11ANCRiSST), Champaign, IL., Champaign, IL., 2015.

[30] J.-O. Lee, T. Kang, K.-H. Lee, S. K. Im, and J. Park, "Vision-based indoor localization for unmanned aerial vehicles," *Journal of Aerospace Engineering,* vol. 24, no. 3, pp. 373-377, 2010.

[31] J. Park, S. Im, K.-H. Lee, and J.-O. Lee, "Vision-based SLAM system for small UAVs in GPS-denied environments," *Journal of Aerospace Engineering,* vol. 25, no. 4, pp. 519-529, 2011.

[32] G. Werner-Allen, K. Lorincz, J. Johnson, J. Lees, and M. Welsh, "Fidelity and yield in a volcano monitoring sensor network," in *Proceedings of the 7th Symposium on Operating Systems Design and Implementation*, 2006, pp. 381-396: USENIX Association.

[33] F. Ye, H. Luo, J. Cheng, S. Lu, and L. Zhang, "A two-tier data dissemination model for large-scale wireless sensor networks," in *Proceedings of the 8th Annual International Conference on Mobile Computing and Networking*, 2002, pp. 148-159: ACM.

[34] E. P. De Freitas *et al.*, "UAV relay network to support WSN connectivity," in *Ultra Modern Telecommunications and Control Systems and Workshops (ICUMT), 2010 International Congress on*, 2010, pp. 309-314: IEEE.

[35] H. Nakayama, N. Ansari, A. Jamalipour, and N. Kato, "Fault-resilient sensing in wireless sensor networks," *Computer Communications,* vol. 30, no. 11, pp. 2375-2384, 2007.

[36] O. Tekdas, V. Isler, J. H. Lim, and A. Terzis, "Using mobile robots to harvest data from sensor fields," *IEEE Wireless Communications,* vol. 16, no. 1, pp. 22-28, 2009.

[37] H. Wei, B. Wang, Y. Wang, Z. Shao, and K. C. Chan, "Staying-alive path planning with energy optimization for mobile robots," *Expert Systems with Applications,* vol. 39, no. 3, pp. 3559-3571, 2012.

[38] E. M. Arkin and R. Hassin, "Approximation algorithms for the geometric covering salesman problem," *Discrete Applied Mathematics,* vol. 55, no. 3, pp. 197-218, 1994.

[39] J. A. Cobano, J. Martínez-de Dios, R. Conde, J. Sánchez-Matamoros, and A. Ollero, "Data retrieving from heterogeneous wireless sensor network nodes using UAVs," *Journal of Intelligent & Robotic Systems,* vol. 60, no. 1, pp. 133-151, 2010.

[40] D. Guimaraes Macharet, A. Alves Neto, V. Fiuza da Camara Neto, and M. Montenegro Campos, "An evolutionary approach for the Dubins' traveling salesman problem with neighborhoods," in *Proceedings of the 14th Annual*

Conference on Genetic and Evolutionary Computation, 2012, pp. 377-384: ACM.

[41] J. T. Isaacs, D. J. Klein, and J. P. Hespanha, "Algorithms for the traveling salesman problem with neighborhoods involving a dubins vehicle," in *American Control Conference (ACC), 2011*, 2011, pp. 1704-1709: IEEE.

[42] B. Yuan, M. Orlowska, and S. Sadiq, "On the optimal robot routing problem in wireless sensor networks," *IEEE Transactions on Knowledge and Data Engineering,* vol. 19, no. 9, pp. 1252-1261, 2007.

[43] Z. Liu, R. Sengupta, and A. Kurzhanskiy, "A power consumption model for multi-rotor small unmanned aircraft systems," in *Unmanned Aircraft Systems (ICUAS), 2017 International Conference on*, 2017, pp. 310-315: IEEE.

[44] C. Toth and G. Jóźków, "Remote sensing platforms and sensors: A survey," *ISPRS Journal of Photogrammetry and Remote Sensing,* vol. 115, pp. 22-36, 2016.

[45] Y. Lin and S. Saripalli, "Sense and avoid for Unmanned Aerial Vehicles using ADS-B," in *Robotics and Automation (ICRA), 2015 IEEE International Conference on*, 2015, pp. 6402-6407: IEEE.

[46] S. Ramasamy and R. Sabatini, "A unified approach to cooperative and non-cooperative Sense-and-Avoid," in *Unmanned Aircraft Systems (ICUAS), 2015 International Conference on*, 2015, pp. 765-773: IEEE.

[47] X. Yu and Y. Zhang, "Sense and avoid technologies with applications to unmanned aircraft systems: Review and prospects," *Progress in Aerospace Sciences,* vol. 74, pp. 152-166, 2015.

[48] J. Chen, Z. Chen, and C. Beard, "Experimental investigation of aerial–ground network communication towards geospatially large-scale structural health monitoring," *Journal of Civil Structural Health Monitoring,* vol. 8, no. 5, pp. 823-832, 2018.

[49] C. A. Trasviña-Moreno, R. Blasco, Á. Marco, R. Casas, and A. Trasviña-Castro, "Unmanned aerial vehicle based wireless sensor network for marine-coastal environment monitoring," *Sensors,* vol. 17, no. 3, p. 460, 2017.

[50] B. Sadeghi, V. Kanodia, A. Sabharwal, and E. Knightly, "Opportunistic media access for multirate ad hoc networks," in *Proceedings of the 8th Annual International Conference on Mobile Computing and Networking*, 2002, pp. 24-35: ACM.

[51] S. Biswas and R. Morris, "ExOR: opportunistic multi-hop routing for wireless networks," in *ACM SIGCOMM Computer Communication Review*, 2005, vol. 35, pp. 133-144: ACM.

[52] T. Small and Z. J. Haas, "Resource and performance tradeoffs in delay-tolerant wireless networks," in *Proceedings of the 2005 ACM SIGCOMM Workshop on Delay-Tolerant Networking*, 2005, pp. 260-267: ACM.

[53] V. Arnaboldi, M. Conti, and F. Delmastro, "Implementation of CAMEO: A context-aware middleware for Opportunistic Mobile Social Networks," in *World of Wireless, Mobile and Multimedia Networks (WoWMoM), 2011 IEEE International Symposium on a*, 2011, pp. 1-3: IEEE.

[54] P. Juang, H. Oki, Y. Wang, M. Martonosi, L. S. Peh, and D. Rubenstein, "Energy-efficient computing for wildlife tracking: Design tradeoffs and early experiences with ZebraNet," *ACM Sigplan Notices,* vol. 37, no. 10, pp. 96-107, 2002.

[55] S. Guo, L. He, Y. Gu, B. Jiang, and T. He, "Opportunistic flooding in low-duty-cycle wireless sensor networks with unreliable links," *Computers, IEEE Transactions on,* vol. 63, no. 11, pp. 2787-2802, 2014.

[56] V. Raghunathan, C. Schurgers, S. Park, and M. B. Srivastava, "Energy-aware wireless microsensor networks," *IEEE Signal Processing Magazine,* vol. 19, no. 2, pp. 40-50, 2002.

[57] J. Polastre, J. Hill, and D. Culler, "Versatile low power media access for wireless sensor networks," in *Proceedings of the 2nd International Conference on Embedded Networked Sensor Systems*, 2004, pp. 95-107: ACM.

[58] W. Ye, J. Heidemann, and D. Estrin, "An energy-efficient MAC protocol for wireless sensor networks," in *INFOCOM 2002. Twenty-First Annual Joint Conference of the IEEE Computer and Communications Societies. Proceedings. IEEE*, 2002, vol. 3, pp. 1567-1576: IEEE.

[59] W. Ye, J. Heidemann, and D. Estrin, "Medium access control with coordinated adaptive sleeping for wireless sensor networks," *IEEE/ACM Trans. Netw.,* vol. 12, no. 3, pp. 493-506, 2004.

[60] T. v. Dam and K. Langendoen, "An adaptive energy-efficient MAC protocol for wireless sensor networks," presented at the Proceedings of the 1st International Conference on Embedded networked Sensor Systems, Los Angeles, California, USA, 2003.

[61] R. Piyare, A. L. Murphy, C. Kiraly, P. Tosato, and D. Brunelli, "Ultra Low Power Wake-Up Radios: A Hardware and Networking Survey," *IEEE Communications Surveys & Tutorials,* vol. 19, no. 4, pp. 2117-2157, 2017.

[62] D. Ye, "A self-adaptive sleep/wake-up scheduling approach for wireless sensor networks," *IEEE Transactions on Cybernetics,* vol. 48, no. 3, pp. 979-992, 2018.

[63] I. Demirkol, C. Ersoy, and E. Onur, "Wake-up receivers for wireless sensor networks: benefits and challenges," *IEEE Wireless Communications,* vol. 16, no. 4, pp. 88-96, 2009.

[64] T. Hakkinen and J. Vanhala, " In Proceedings of the 4th International Conference on Intelligent Environments (IE), Seattle, USA, 21 Jul 2008; pp. 1-4.

[65] J. Han, C. s. Choi, and I. Lee, "More efficient home energy management system based on ZigBee communication and infrared remote controls," *IEEE Transactions on Consumer Electronics,* vol. 57, no. 1, pp. 85-89, 2011.

[66] G. Kim *et al.*, "A 695 pW standby power optical wake-up receiver for wireless sensor nodes," in *Custom Integrated Circuits Conference (CICC), 2012 IEEE*, 2012, pp. 1-4: IEEE.

[67] J. Mathews, M. Barnes, A. Young, and D. Arvind, "Low power wake-up in wireless sensor networks using free space optical communications," in *Sensor Technologies and Applications (SENSORCOMM), 2010 Fourth International*

Conference on, 2010, pp. 256-261: IEEE.

[68] F. Hoflinger, G. U. Gamm, J. Albesa, and L. M. Reindl, "Smartphone remote control for home automation applications based on acoustic wake-up receivers," in *Instrumentation and Measurement Technology Conference (I2MTC) Proceedings, 2014 IEEE International*, 2014, pp. 1580-1583: IEEE.

[69] A. Sánchez, S. Blanc, P. Yuste, A. Perles, and J. J. Serrano, "An ultra-low power and flexible acoustic modem design to develop energy-efficient underwater sensor networks," *Sensors,* vol. 12, no. 6, pp. 6837-6856, 2012.

[70] K. Yadav, I. Kymissis, and P. R. Kinget, "A 4.4-$\mu $ W Wake-Up Receiver Using Ultrasound Data," *IEEE Journal of Solid-State Circuits,* vol. 48, no. 3, pp. 649-660, 2013.

[71] E. Lattanzi, M. Dromedari, V. Freschi, and A. Bogliolo, "A sub-a ultrasonic wake-up trigger with addressing capability for wireless sensor nodes," *ISRN Sensor Networks,* vol. 2013, 2013.

[72] J. C. Jackson, R. Summan, G. I. Dobie, S. M. Whiteley, S. G. Pierce, and G. Hayward, "Time-of-flight measurement techniques for airborne ultrasonic ranging," *IEEE Transactions on Ultrasonics, Ferroelectrics, and Frequency Control,* vol. 60, no. 2, pp. 343-355, 2013.

[73] W. Jiang and W. M. Wright, "Indoor airborne ultrasonic wireless communication using OFDM methods," *IEEE Transactions on Ultrasonics, Ferroelectrics, and Frequency Control,* vol. 64, no. 9, pp. 1345-1353, 2017.

[74] H. Kim *et al.*, "CMOS passive wake-up circuit for sensor network applications," *Microwave and Optical Technology Letters,* vol. 52, no. 3, pp. 597-600, 2010.

[75] C. Chung, Y.-H. Kim, T.-H. Ki, K. Bae, and J. Kim, "Fully integrated ultra-low-power 900 MHz RF transceiver for batteryless wireless microsystems," in *Electronics, Circuits and Systems (ICECS), 2011 18th IEEE International Conference on*, 2011, pp. 196-199: IEEE.

[76] P. Kamalinejad, K. Keikhosravy, M. Magno, S. Mirabbasi, V. C. Leung, and L. Benini, "A high-sensitivity fully passive wake-up radio front-end for wireless sensor nodes," in *Consumer Electronics (ICCE), 2014 IEEE International Conference on*, 2014, pp. 209-210: IEEE.

[77] L. Gu and J. A. Stankovic, "Radio-Triggered Wake-Up for Wireless Sensor Networks," *Real-Time Systems,* vol. 29, no. 2, pp. 157-182, 2005.

[78] L. Chen *et al.*, "Range extension of passive wake-up radio systems through energy harvesting," in *2013 IEEE International Conference on Communications (ICC)*, 2013, pp. 1549-1554.

[79] L. Chen *et al.*, "Reach2-Mote: A Range-Extending Passive Wake-Up Wireless Sensor Node," *ACM Trans. Sen. Netw.,* vol. 11, no. 4, pp. 1-33, 2015.

[80] L. Chen, J. Warner, W. Heinzelman, and I. Demirkol, "MH-REACH-Mote: Supporting multi-hop passive radio wake-up for wireless sensor networks," In Proceedings of the 2015 IEEE International Conference on Communications (ICC), vol. 2015, pp. 6512-6518.

[81] H. Ba, I. Demirkol, and W. Heinzelman, "Feasibility and benefits of passive RFID wake-up radios for wireless sensor networks," in *Global*

Telecommunications Conference (GLOBECOM 2010), 2010 IEEE, 2010, pp. 1-5: IEEE.

[82] H. Ba, I. Demirkol, and W. Heinzelman, "Passive wake-up radios: From devices to applications," *Ad Hoc Networks,* vol. 11, no. 8, pp. 2605-2621, 2013.

[83] C. Petrioli, D. Spenza, P. Tommasino, and A. Trifiletti, "A novel wake-up receiver with addressing capability for wireless sensor nodes," in *Distributed Computing in Sensor Systems (DCOSS), 2014 IEEE International Conference on*, 2014, pp. 18-25: IEEE.

[84] N. M. Pletcher, S. Gambini, and J. Rabaey, "A 52$\mu $ W Wake-Up Receiver With $-$72 dBm Sensitivity Using an Uncertain-IF Architecture," *IEEE Journal of Solid-State Circuits,* vol. 44, no. 1, pp. 269-280, 2009.

[85] M. Magno, V. Jelicic, B. Srbinovski, V. Bilas, E. Popovici, and L. Benini, "Design, implementation, and performance evaluation of a flexible low-latency nanowatt wake-up radio receiver," *IEEE Transactions on Industrial Informatics,* vol. 12, no. 2, pp. 633-644, 2016.

[86] J. Oller, I. Demirkol, J. Casademont, and J. Paradells, "Design, development, and performance evaluation of a low-cost, low-power wake-up radio system for wireless sensor networks," *ACM Transactions on Sensor Networks (TOSN),* vol. 10, no. 1, p. 11, 2013.

[87] J. Oller *et al.*, "IEEE 802.11-enabled wake-up radio system: Design and performance evaluation," *Electronics Letters,* vol. 50, no. 20, pp. 1484-1486, 2014.

[88] J. Oller, I. Demirkol, J. Casademont, J. Paradells, G. U. Gamm, and L. Reindl, "Performance evaluation and comparative analysis of subcarrier modulation wake-up radio systems for energy-efficient wireless sensor networks," *Sensors,* vol. 14, no. 1, pp. 22-51, 2013.

[89] S. Bdiri and F. Derbel, "An Ultra-Low Power Wake-Up Receiver for Realtime constrained Wireless Sensor Networks," in *AMA Conferences Nürnberg, Germany, Proceedings SENSOR 2015, D6-Sensor Electronic*, 2015, pp. 612-617.

[90] F. Sutton, B. Buchli, J. Beutel, and L. Thiele, "Zippy: On-demand network flooding," in *Proceedings of the 13th ACM Conference on Embedded Networked Sensor Systems*, 2015, pp. 45-58: ACM.

[91] M. Prinn, L. Moore, M. Hayes, and B. O'Flynn, "Comparing low power listening techniques with wake-up receiver technology," in *Proceedings of SMART*, 2014, pp. 20-24.

[92] Libelim. (2018). *Waspmote - Open Source Sensor Node for the Internet of Things*. Available: http://www.libelium.com/products/waspmote/

[93] H. Milosiu, F. Oehler, and M. Eppel, "Sub-10 µA data reception with low latency using a 180-nm CMOS wake-up receiver at 868 MHz," in *Semiconductor Conference Dresden (SCD), 2011*, 2011, pp. 1-4: IEEE.

[94] T. Kumberg, R. Tannhaeuser, G. Gamm, and L. Reindl, "Energy improved wake-up strategy for wireless sensor networks," in *Sensors and Measuring Systems 2014; 17. ITG/GMA Symposium; Proceedings of*, 2014, pp. 1-6: VDE.

[95] ASCE. (2017). *ASCE's 2017 Infrastructure Report Card (D+)*. Available: https://www.infrastructurereportcard.org/

[96] J. Zhao and J. T. DeWolf, "Dynamic monitoring of steel girder highway bridge," *Journal of Bridge Engineering,* vol. 7, no. 6, pp. 350-356, 2002.

[97] H. Yoon, J. Shin, and B. F. Spencer Jr, "Structural Displacement Measurement using an Unmanned Aerial System," *Computer-Aided Civil and Infrastructure Engineering,* vol. 33, no. 3, pp. 183-192, 2018.

[98] H. Yoon, V. Hoskere, J.-W. Park, and B. F. Spencer, "Cross-correlation-based structural system identification using unmanned aerial vehicles," *Sensors,* vol. 17, no. 9, p. 2075, 2017.

[99] F. Moreu, P. Garg, and E. Ayorinde, "Railroad Bridge Inspections for Maintenance and Replacement Prioritization Using Unmanned Aerial Systems (UAS) with Laser Capabilities," 2018.

[100] B. Spencer Jr, J.-W. Park, K. Mechitov, H. Jo, and G. Agha, "Next generation wireless smart sensors toward sustainable civil infrastructure," *Procedia Engineering,* vol. 171, pp. 5-13, 2017.

[101] S. Tang and Z. Chen, "Level-of-detail Assessment of Structural Surface Damage using Spatially Sequential Stereo Images and Deep Learning Methods," presented at the The 11th International Workshop on Structural Health Monitoring, Stanford, CA, USA, 2017.

[102] S.-H. Sim, J. F. Carbonell-Márquez, B. Spencer Jr, and H. Jo, "Decentralized random decrement technique for efficient data aggregation and system identification in wireless smart sensor networks," *Probabilistic Engineering Mechanics,* vol. 26, no. 1, pp. 81-91, 2011.

[103] S.-H. Sim, B. Spencer Jr, M. Zhang, and H. Xie, "Automated decentralized modal analysis using smart sensors," *Structural Control and Health Monitoring,* vol. 17, no. 8, pp. 872-894, 2010.

[104] J. Hou, B. Chang, D.-K. Cho, and M. Gerla, "Minimizing 802.11 interference on ZigBee medical sensors," in *Proceedings of the Fourth International Conference on Body Area Networks*, 2009, p. 5: ICST (Institute for Computer Sciences, Social-Informatics and Telecommunications Engineering).

[105] J. Huang, G. Xing, G. Zhou, and R. Zhou, "Beyond co-existence: Exploiting WiFi white space for Zigbee performance assurance," in *Network Protocols (ICNP), 2010 18th IEEE International Conference on*, 2010, pp. 305-314: IEEE.

[106] C.-J. M. Liang, N. B. Priyantha, J. Liu, and A. Terzis, "Surviving wi-fi interference in low power zigbee networks," in *Proceedings of the 8th ACM Conference on Embedded Networked Sensor Systems*, 2010, pp. 309-322: ACM.

[107] R. Xu, G. Shi, J. Luo, Z. Zhao, and Y. Shu, "Muzi: Multi-channel zigbee networks for avoiding wifi interference," in *Internet of Things (IThings/CPSCom), 2011 International Conference on and 4th International Conference on Cyber, Physical and Social Computing*, 2011, pp. 323-329: IEEE.

[108] X. Zhang and K. G. Shin, "Enabling coexistence of heterogeneous wireless

systems: Case for ZigBee and WiFi," in *Proceedings of the Twelfth ACM International Symposium on Mobile Ad Hoc Networking and Computing*, 2011, p. 6: ACM.

[109] S. Y. Shin, H. S. Park, S. Choi, and W. H. Kwon, "Packet error rate analysis of ZigBee under WLAN and Bluetooth interferences," *IEEE Transactions on Wireless Communications,* vol. 6, no. 8, 2007.

[110] P. Yi, A. Iwayemi, and C. Zhou, "Developing ZigBee deployment guideline under WiFi interference for smart grid applications," *IEEE Transactions on Smart Grid,* vol. 2, no. 1, pp. 110-120, 2011.

[111] G. Thonet, P. Allard-Jacquin, and P. Colle, "Zigbee-wifi coexistence," *Schneider Electric White Paper and Test Report,* vol. 1, pp. 1-38, 2008.

[112] S. Kemkemian, M. Nouvel-Fiani, P. Cornic, P. Le Bihan, and P. Garrec, "Radar systems for "Sense and Avoid" on UAV," in *Radar Conference-Surveillance for a Safer World, 2009. RADAR. International*, 2009, pp. 1-6: IEEE.

[113] Y. Watanabe, A. Calise, and E. Johnson, "Vision-based obstacle avoidance for UAVs," in *AIAA Guidance, Navigation and Control Conference and Exhibit*, 2007, p. 6829.

[114] A. Dumitrescu and J. S. Mitchell, "Approximation algorithms for TSP with neighborhoods in the plane," *Journal of Algorithms,* vol. 48, no. 1, pp. 135-159, 2003.

[115] X. Zhang, J. Chen, B. Xin, and Z. Peng, "A memetic algorithm for path planning of curvature-constrained UAVs performing surveillance of multiple ground targets," *Chinese Journal of Aeronautics,* vol. 27, no. 3, pp. 622-633, 2014.

[116] A. Boukerche and A. Darehshoorzadeh, "Opportunistic routing in wireless networks: Models, algorithms, and classifications," *ACM Computing Surveys (CSUR),* vol. 47, no. 2, p. 22, 2015.

[117] D. Rosario, Z. Zhao, T. Braun, E. Cerqueira, A. Santos, and I. Alyafawi, "Opportunistic routing for multi-flow video dissemination over flying ad-hoc networks," in *2014 IEEE 15th International Symposium on*, 2014, pp. 1-6: IEEE.

[118] D. Rosário, Z. Zhao, A. Santos, T. Braun, and E. Cerqueira, "A beaconless opportunistic routing based on a cross-layer approach for efficient video dissemination in mobile multimedia IoT applications," *Computer Communications,* vol. 45, pp. 21-31, 2014.

[119] A. Dumitrescu and JSB. Mitchell, "Approximation algorithms for TSP with neighborhoods in the plane," *Journal of Algorithms,* vol. 48, no. 1, pp. 135-159, 2003.

[120] J. Gudmundsson and C. Levcopoulos, "A fast approximation algorithm for TSP with neighborhoods," *Journal of Algorithms,* vol. 6, no. 4, pp. 469-488, 1999.

[121] M. de Berg, J. Gudmundsson, M. J. Katz, C. Levcopoulos, M. H. Overmars, and A. van der Stappen, "TSP with neighborhoods of varying size," *Journal of Algorithms,* vol. 57, no. 1, pp. 22-36, 2005.

[122] K. Elbassioni, A. V. Fishkin, and R. Sitters, "Approximation algorithms for the Euclidean traveling salesman problem with discrete and continuous

neighborhoods," *International Journal of Computational Geometry & Applications,* vol. 19, no. 02, pp. 173-193, 2009.

[123] J. Gudmundsson and C. Levcopoulos, "A fast approximation algorithm for TSP with neighborhoods and red-blue separation," in *International Computing and Combinatorics Conference*, 1999, pp. 473-482: Springer.

[124] C. Tunca, S. Isik, M. Y. Donmez, and C. Ersoy, "Distributed mobile sink routing for wireless sensor networks: A survey," vol. 16, no. 2, pp. 877-897, 2014.

[125] M. Gündüz, M. S. Kiran, and E. Özceylan, "A hierarchic approach based on swarm intelligence to solve the traveling salesman problem," *Turkish Journal of Electrical Engineering & Computer Sciences,* vol. 23, no. 1, pp. 103-117, 2015.

[126] A. Ouaarab, B. Ahiod, and X. Yang, "Discrete cuckoo search algorithm for the travelling salesman problem," *Neural Computing and Applications,* vol. 24, no. 7-8, pp. 1659-1669, 2014.

[127] S. Burer, A. Letchford, and M. Science, "Non-convex mixed-integer nonlinear programming: A survey," Surveys in Operations Research and Management Science. vol. 17, no. 2, pp. 97-106, 2012.

[128] I. Gentilini, F. Margot, and K. Shimada "The travelling salesman problem with neighbourhoods: MINLP solution," Optimization Methods and Software, vol. 28, no. 2, pp. 364-378, 2013.

[129] K. Vicencio, B. Davis, and I. Gentilini, "Multi-goal path planning based on the generalized traveling salesman problem with neighborhoods," in *Intelligent Robots and Systems (IROS 2014), 2014 IEEE/RSJ International Conference on*, 2014, pp. 2985-2990: IEEE.

[130] T. M. Chiwewe and G. Hancke, "A distributed topology control technique for low interference and energy efficiency in wireless sensor networks," *IEEE Transactions on Industrial Informatics*, vol. 8, no. 1, pp. 11-19, 2012.

[131] A. Terzis, "Minimising the effect of WiFi interference in 802.15. 4 wireless sensor networks," *International Journal of Sensor Networks,* vol. 3, no. 1, pp. 43-54, 2007.

[132] G. Zhou, T. He, J. A. Stankovic, and T. Abdelzaher, "RID: Radio interference detection in wireless sensor networks," in *INFOCOM 2005. 24th Annual joint conference of the IEEE Computer and Communications Societies. Proceedings IEEE*, 2005, vol. 2, pp. 891-901: IEEE.

[133] O. Kröger, C. Coffrin, H. Hijazi, and H. Nagarajan, "Juniper: An Open-Source Nonlinear Branch-and-Bound Solver in Julia," in *International Conference on the Integration of Constraint Programming, Artificial Intelligence, and Operations Research*, 2018, pp. 377-386: Springer.

VITA

Jianfei Chen was born on April 23, 1987, in Chongqing, China. He received his Bachelor's degree in Telecommunication from University of Beijing Post and Communications, Beijing, China in 2010.

Jianfei received his Master of Science degree at University of Missouri-Kansas City in 2013 and continued pursued an Interdisciplinary PhD degree at the same University. His primary PhD discipline is Electrical and Computer Engineering. His co-discipline is Engineering. His research interests include remote sensing, wireless sensing network, system integration and embedded system.